Inorganic Chemistry
Cite This: Inorg. Chem. XXXX, XXX, XXX–XXX
Article
pubs.acs.org/IC

The Thiolate Trans Effect in Heme {FeNO}^{6} Complexes and Beyond: Insight into the Nature of the Push Effect

Andrew P. Hunt and Nicolai Lehnert*

Department of Chemistry, University of Michigan, 930 North University Avenue, Ann Arbor, Michigan 48109, United States

Supporting Information

ABSTRACT: Cyt P450 nitric oxide (NO) reductase (P450nor) is an important enzyme in fungal denitrification, responsible for the large-scale production of the greenhouse gas N_2O. In the first step of catalysis, the ferric heme-thiolate active site of P450nor binds NO to produce a ferric heme-nitrosyl or {FeNO}^{6} intermediate (in the Enemark–Feltham notation). In this paper, we present the low-temperature preparation of six new heme-thiolate {FeNO}^{6} model complexes, [Fe(TPP)(SPh*)(NO)], using a unique series of electron-poor thiophenolates (SPh*$^-$), and their detailed spectroscopic characterization. Our data show experimentally, for the first time, that a direct correlation exists between the thiolate donor strength and the Fe–NO and N–O bond strengths, evident from the corresponding stretching frequencies. This is due to a σ-trans effect of the thiolate ligand, which manifests itself in the population of an Fe–N–O σ-antibonding (σ^*) orbital. Via control of the thiolate donor strength (using hydrogen bonds), nature is therefore able to exactly control the degree of activation of the FeNO unit in P450nor. Vice versa, NO can be used as a sensitive probe to quantify the donor strength of a thiolate ligand in a model system or protein, by simply measuring the Fe–NO and N–O frequencies of the ferric NO adduct and then projecting those data onto the correlation plot established here. Finally, we are able to show that the σ-trans effect of the thiolate is the electronic origin of the "push" effect, which is proposed to mediate O–O bond cleavage and Compound I formation in Cyt P450 monooxygenase catalysis.

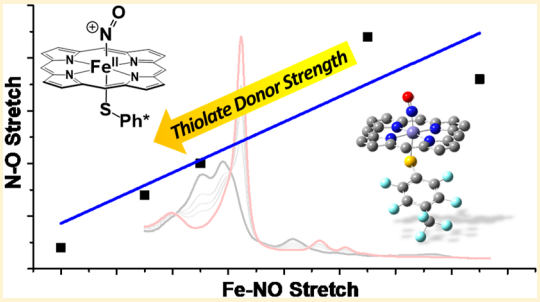

INTRODUCTION

Nitric oxide (NO) is well recognized as an important intercellular signaling molecule that is involved in blood pressure control and nerve signal transduction in humans and other mammals at nanomolar concentrations.[1] At increased micromolar concentrations, however, NO is toxic to most organisms, resulting in nitrosative stress, which can cause detrimental health conditions such as nerve damage, organ degradation, and cartilage disintegration, to name a few.[1] NO is also a key component of septic shock.[2] Owing to the important functions and the potential threats NO poses, the presence of different enzymes that mediate its production, regulation, and detoxification is crucial in biological systems.[3] One such enzyme, cytochrome P450 nitric oxide reductase (P450nor), is utilized by soil-dwelling fungi during denitrification, which is an anaerobic form of respiration where nitrate (NO_3^-) and nitrite (NO_2^-) are stepwise reduced to nitrous oxide (N_2O).[4] In these organisms, P450nor catalyzes the reduction of NO to N_2O in order to prevent the accumulation of this toxic metabolite,[5] according to the following overall equation: $2\,NO + 2e^- + 2\,H^+ \rightarrow N_2O + H_2O$. The product of fungal denitrification, N_2O, is a potent greenhouse gas, which in turn contributes to the effects of global warming, with a 100 year warming potential approximately 300 times higher than that of CO_2.[6] N_2O is also an ozone-depleting agent. As farmers in the developed world tend to overfertilize their agricultural soils, denitrification and N_2O production are stimulated, with ~75% of the atmospheric N_2O now being linked to agriculture.[6] On the basis of these circumstances, there is currently a great interest in determining the sources of N_2O emissions from soils and in elucidating the mechanisms of the bacterial and fungal enzymes that catalyze its production. In this regard, P450nor is the key fungal enzyme responsible for N_2O generation, and it is currently the subject of intense scientific investigations.[7−10]

Analogous to other members of the cytochrome P450 (Cyt P450) enzyme family, the central features of the P450nor active site are the presence of an iron porphyrin, heme *b* center, with a proximally bound, deprotonated cysteinate (thiolate) ligand (Figure 1).[5,11,12] The presence of the thiolate ligand is central to catalysis for Cyt P450s and presents a hallmark of their active sites. Additionally, these enzymes contain conserved active site residues around the proximal cysteinate ligand which form hydrogen bonds (H-bonds) with the sulfur atom (see Figure 1), making up what is referred to as the Cys pocket. These H-bonds are proposed to play important roles in fine tuning the reactivity of the heme Fe for the desired catalytic reaction[13] and for stabilizing the thiolate ligand to prevent undesired side reactions, for example protonation or reaction with O_2 or NO, which would lead to enzyme deactivation.[14] Two particular roles for the thiolate

Received: January 10, 2019

DOI: 10.1021/acs.inorgchem.9b00091
Inorg. Chem. XXXX, XXX, XXX–XXX

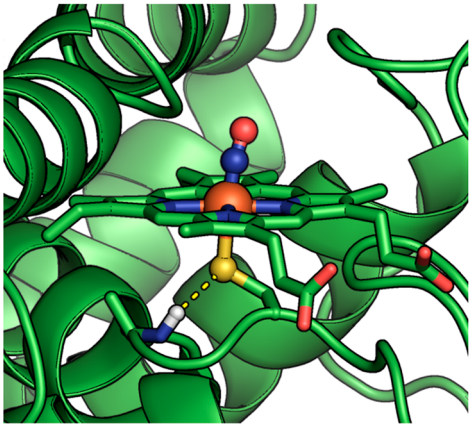

Figure 1. Crystal structure of the Cyt P450nor ferric heme-nitrosyl complex (PDB code: 1CL6).[2] The strongest hydrogen bond to the proximally bound cysteinate (thiolate) ligand from the amide backbone is shown as a yellow dashed line. The other two H-bonds present in the P450nor Cys pocket have been omitted for clarity.

ligand in the Cyt P450 catalytic cycle have been identified: (a) the so-called "push effect", where it has been proposed that the electron donation from the thiolate accelerates O−O bond cleavage in the hydroperoxo intermediate,[15] and (b) the increase in the basicity of Compound II,[16] which assists in the H atom abstraction step central to the reaction of many Cyt P450s.

In the mechanism of P450nor, the ferric heme-thiolate resting state binds 1 equivalent (equiv) of NO to form a ferric heme-nitrosyl complex,[17] which constitutes the first key intermediate of the reaction. This species subsequently reacts with NAD(P)H directly (by abstracting a hydride) to form a ferrous HNO complex.[18] Either this species or the corresponding, protonated species that contains an axial $[Fe\text{-}NHOH]^{3+}$ unit constitutes the key "Intermediate *I*", which is then reactive toward the second molecule of NO and induces N−N bond formation and N_2O generation. DFT calculations predict that the initially formed HNO ligand is quite basic, due to the presence of the strongly donating, proximal cysteinate ligand and therefore becomes protonated,[19,7] which would identify the (formally) hydroxylamide ($HNOH^-$) adduct as Intermediate *I*. However, the true nature and electronic structure of Intermediate *I* is currently unknown, due to limited characterization of this short-lived species in the enzyme.

To elucidate the mechanism and gain a better understanding of how the P450nor active site is tailored for NO reduction, we use synthetic model complexes to determine the geometric and electronic properties associated with the reactive species involved in P450nor catalysis. Specifically, in this work we model the first step in the P450nor mechanism in which NO binds to the ferric heme resting state, generating a thiolate-coordinated ferric heme-nitrosyl or $\{FeNO\}^6$ complex in the Enemark−Feltham notation[20] (Figure 1), where the superscript "6" represents the sum of the electrons in the Fe(d) and NO(π^*) orbitals. Since NO is a "noninnocent" (or redox-active) ligand, this notation is useful for keeping track of the oxidation state of the Fe−N−O unit, without having to be specific about the exact electron distribution in a given complex. For example, while heme $\{FeNO\}^6$ complexes are referred to as ferric heme-nitrosyls, spectroscopic studies have concluded that the Fe−N−O unit is actually best described as having an $Fe^{II}-NO^+$ electronic structure.[21−23] This electronic description is reflected by the reactivity of the P450nor $\{FeNO\}^6$ complex, where the formally NO^+ ligand is electrophilic, which explains its ability to abstract a hydride from NAD(P)H to ultimately generate Intermediate *I*.

One important question in this regard is how the thiolate ligand affects the geometric and electronic structure of the $\{FeNO\}^6$ unit and how this relates to catalysis. Whereas imidazole-coordinated $\{FeNO\}^6$ complexes in model systems and proteins (especially globins have been investigated) show linear Fe−N−O units and N−O and Fe−NO stretching frequencies in the 1900−1920 and ∼590 cm^{-1} ranges,[24] respectively, interesting deviations from these properties have been observed in the presence of axial thiolate coordination, but the electronic−structural reasons for these deviations are currently unknown. For example, the crystal structure of the P450nor $\{FeNO\}^6$ complex displays a bent Fe−N−O unit with an angle of 161°,[5] and the N−O and Fe−NO stretching modes are observed at 1851 and 530 cm^{-1}, respectively, for this enzyme.[25] The $\{FeNO\}^6$ complexes of other heme-thiolate enzymes have also been successfully generated, including Cyt P450cam, chloroperoxidase (CPO), and nitric oxide synthase (NOS), which show overall similar properties.[26−29] Computational work has further indicated that there is a direct correlation between the thiolate donor strength and the strengths of the Fe−NO and N−O bonds (evident from the corresponding stretching frequencies).[21] However, other than computational results, no experimental data are available that *directly* probe the relation between the thiolate donor strength and the properties of the Fe−N−O unit in thiolate-coordinated $\{FeNO\}^6$ complexes. In this regard, making comparisons between different proteins is problematic, since the active sites of different proteins also differ greatly in (a) the exact environment of the cysteinate axial ligand and the heme, (b) heme distortions, and (c) steric restrictions in the active site, which makes it difficult to derive exact trends from these data. This is a scientific question that is ideally addressed with model complexes, but past studies have shown that thiolate-coordinated $\{FeNO\}^6$ complexes are extremely unstable, and in fact, only two corresponding model complexes have been reported, with limited characterization available.[30−32] The data presented in this study fill this void and provide, for the first time, experimental data for a series of model complexes, [Fe(TPP)(SR)(NO)] (TPP = tetraphenylporphyrin dianion), where the exact same porphyrin ligand is used and only the donor strength of the axial thiolate ligand (SR^-) is varied. This is accomplished by using a series of thiophenolates (SPh^{*-}) that contain different electron-withdrawing substituents (see Scheme 1). The corresponding $\{FeNO\}^6$ complexes are again very unstable but, as we demonstrate here, can be prepared at low temperature (−80 °C) and then studied using IR and resonance Raman spectroscopy. In this way, we are able to establish the direct correlation between the thiolate donor strength and the Fe−NO and N−O bond strengths, which implies that the thiolate ligand imparts a σ-trans effect (interaction) on the Fe−N−O unit. This effect is then further analyzed using DFT calculations. On the basis of the ν(Fe−NO)/ν(N−O) correlation that we establish here, it is now possible to quantify the donor strength of a thiolate (in model systems and new Cyt P450 enzymes) by simply binding NO to the ferric form of the complex and then determining the Fe−NO and N−O stretching frequencies. Finally, we investigated whether a similar thiolate σ-trans effect is at work in the ferric

DOI: 10.1021/acs.inorgchem.9b00091
Inorg. Chem. XXXX, XXX, XXX−XXX

Scheme 1. Series of Thiophenolate Ligands (SPh*$^-$) Used in This Work to Prepare Ferric Heme-Thiolate Complexes, in Order of Decreasing Donor Strength (from Left to Right)[a]

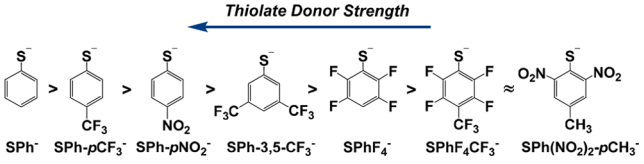

[a]The order in thiolate donor strength to the heme indicated here is largely based on experimental thiol/thiolate pK_a values (SPh$^-$, 6.62;[66] SPh-pNO_2^-, 4.72;[66] SPhF_4^-, 2.75[67]) and the results of the DFT calculations shown in Table 2.

heme-hydroperoxo intermediate in Cyt P450s that would provide an orbital-based explanation for the "push" effect of the thiolate (which assists in O−O bond cleavage), as proposed by Dawson.[15] These results are summarized in this paper.

EXPERIMENTAL SECTION

General Methods. The preparation, handling, and reaction of all O_2- and H_2O-sensitive materials was carried out under inert conditions (N_2 or Ar gas) using standard Schlenk techniques or in an N_2-atmosphere MBraun glovebox equipped with a circulating purifier (O_2, H_2O <0.1 ppm). All reagents were purchased from commercial sources (Fisher Scientific, Sigma-Aldrich, Acros Organics, Alfa Aesar, Cambridge Isotope Laboratories Inc.) and were used as received, unless noted below. Nitric oxide (Cryogenic Gases Inc., 99.5%) was purified by passage through an Ascarite II column (NaOH on silica) followed by a cold trap at −80 °C to remove higher-order nitrogen oxide impurities. $^{15}N^{18}O$-labeled nitric oxide (Sigma-Aldrich) was used without further purification. All solvents used here were distilled from CaH_2 under N_2, degassed via five freeze−pump−thaw cycles, and stored over appropriately sized (3 or 4 Å) activated molecular sieves in a glovebox until used. All low-temperature experiments and sample preparations were carried out in a glovebox cold well, externally cooled by the use of dry ice/acetone, or liquid N_2 as needed to reach the desired temperature. [Fe(TPP)(Cl)] was synthesized as previously reported.[33]

Physical Measurements. *UV−Vis Spectroscopy.* All UV−vis spectra were recorded using an Analytik Jena Specord S600 spectrometer. In situ dip probe experiments were carried out with the same spectrometer connected through a fiber optics cable to a Hellma Analytics Excalibur Standard All-Quartz Immersion Probe with a 10 mm path length (Model 661-202-10-S-46). The temperature of the solution for low-temperature UV−vis dip probe experiments was directly monitored by use of an Omega HH91 Digital Thermometer equipped with a PFA Coated Thermocouple Probe.

IR Spectroscopy. All IR spectra were taken on a Bruker Alpha-E FTIR spectrometer. Solution samples were measured in a thin-layer solution cell equipped with CaF_2 windows.

NMR Spectroscopy. Proton and fluorine NMR spectra were recorded on a Varian MR 400 MHz instrument or a Varian NMRS 500 or 700 MHz spectrometer at room temperature (typically 20−22 °C). All spectra were referenced to internal solvent peaks (e.g., benzene-d_6 at 7.16 ppm).

EPR Spectroscopy. Electron paramagnetic resonance (EPR) spectra were recorded on a Bruker X-band EMX spectrometer equipped with Oxford Instruments liquid-nitrogen and liquid-helium cryostats. EPR spectra were typically obtained on frozen-solution samples (∼1−2 mM) using 20 mW microwave power and 100 kHz field modulation with the amplitude set to 1 G. EPR spectra were fit to determine the g values and degree of rhombicity (E/D) using the program SpinCount (by Prof. M. P. Hendrich, Carnegie Mellon University). For all simulations, a D value of 7 cm^{-1} was used, as the D values of other high-spin ferric heme-thiolate complexes have been reported to vary roughly between 5 and 10 cm^{-1}.[34,35]

Resonance Raman Spectroscopy. Resonance Raman (rRaman) measurements were performed using the 458 nm excitation line from a mixed gas Kr−Ar Coherent Innova 70C Spectrum laser or the 457 nm excitation line from a Cobolt 08-DPL diode pumped laser, on 1/1 CH_2Cl_2/toluene frozen glass samples in liquid N_2. For measurements with the 458 nm laser, the scattered light was collected at a 135° backscattering geometry by a 55 mm FD f/1.2 mounted Canon lens and focused onto the 100 μm entrance slit of a spectrograph using a Newport Corporation 50 mm, f/4 achromatic lens. Rayleigh scattering was rejected by use of a Semrock RazorEdge long-pass edge filter. The Raman scattered light was dispersed in an f/4.6, 0.32 m imaging spectrograph (Princeton Instruments, IsoPlane SCT 320) equipped with an 1800 gr/mm holographic grating and imaged onto a Peltier-cooled CCD detector (Princeton Instruments, Pixis 100B). For data collection with the 457 nm laser, the scattered light was focused onto an Acton two-stage TriVista 555 monochromator and detected by a liquid-N_2-cooled Princeton Instruments Spec-10:400B/LN CCD camera. Samples were prepared at a concentration of 2 mM, and the laser power was adjusted to 10 mW or lower for data collection of the heme-thiolate {FeNO}^{6} samples to prevent NO photolysis. Single-pixel spikes due to cosmic rays recorded by the detector were removed manually from the spectra after data collection. All spectra were calibrated to the toluene peaks at 522 and 623 cm^{-1} (see Figure S8) as an internal standard.

Syntheses. *Synthesis of [Fe(TPP)(OCH$_3$)].* This complex has been previously reported and was prepared using a modified procedure developed here which differs from that reported by Sato and co-workers.[36,37] In the glovebox, 1.05 g (1.49 mmol) of [Fe(TPP)(Cl)] and 323 mg (5.98 mmol) of $NaOCH_3$ were dissolved in approximately 125 mL of CH_2Cl_2 and 12 mL of anhydrous methanol. The solution was vigorously stirred for 1 h, at which time the solution changed color from dark brown to dark green. The reaction mixture was then tested by UV−vis, which indicated complete conversion of the chloro complex to [Fe(TPP)(OCH_3)]. All solvent was then removed under reduced pressure with gentle heating on a Schlenk line, resulting in a purple solid. Once it was returned to the glovebox, the solid was again dissolved in CH_2Cl_2 and filtered through a frit by vacuum filtration to remove insoluble salts. All solvent was then removed, resulting in a dark purple solid. The solid was then suspended in anhydrous methanol and collected on a frit by vacuum filtration, washed with additional, fresh methanol to ensure removal of any excess $NaOCH_3$ followed by washing with hexanes, and finally dried under vacuum. Yield: 988 mg (1.41 mmol, 94% yield). UV−vis (CH_2Cl_2): 416, 578, 630 nm. ^{1}H NMR (C_6D_6): 80.78 (br, β-pyrrole H), 10.59 (s, *m*-Ph), 9.82 (s, o-Ph), 6.66 (br, *p*-Ph). Anal. Calcd for $C_{45}H_{31}FeN_4O$: C, 77.26; H, 4.47; N, 8.01. Found: C, 77.13; H, 4.31; N, 7.91; Cl, 0.0.

General Procedure for the Synthesis of [Fe(TPP)(SPh)] Complexes.* In the glovebox, [Fe(TPP)(OCH_3)] (typically 50−100 mg) was mixed with 1.05 equiv of the desired thiol in dry CH_2Cl_2, resulting in an acid/base ligand exchange between the basic methoxide ligand and the more acidic thiol, generating the desired ferric heme-thiolate complex and methanol as the only byproduct. Upon addition of the thiol, the dark green solution of [Fe(TPP)(OCH_3)] changed color to dark brown-red. The reaction was monitored by UV−vis spectroscopy to determine when the reaction had gone to completion, which was extremely quickly (the color change was visually complete within the mixing time; less than 1 min by UV−vis spectroscopy). Once the reaction was completed, all solvent was removed via reduced pressure on a Schlenk line. The product was then collected on a frit inside the glovebox via vacuum filtration by suspending the resulting solid in a mixture of hexanes and methanol (3/1). The collected solid was then washed with additional methanol, followed by hexanes, and dried under reduced pressure. The product was tested by UV−vis and NMR spectroscopy to ensure purity. If necessary, the product was further purified by recrystallization by dissolving it in a minimal amount of CH_2Cl_2, layering the

DOI: 10.1021/acs.inorgchem.9b00091
Inorg. Chem. XXXX, XXX, XXX−XXX

solution with hexanes, and placing it in a freezer overnight. Of the ferric heme-thiolate complexes prepared and studied here, [Fe(TPP)(SPhF$_4$)],[38] [Fe(TPP)(SPh-*p*NO$_2$)],[39,40] and [Fe(TPP)(SPh)][41−43] have been previously reported (see references).

Synthesis of [Fe(TPP)(SPhF$_4$CF$_3$)]. UV−vis: (toluene) 384, 413, 516, 578, 607, 675, 716 nm; (CH_2Cl_2) 380, 413, 516, 581, 608, 673, 717 nm. ^{1}H NMR (C_6D_6): 71.8 (br, β-pyrrole H), 13.2 and 11.9 (d, meta-Ph TPP), 9.0 and 5.8 (br, ortho-Ph TPP), 6.4 (s, para-Ph TPP) ppm. ^{19}F NMR (C_6D_6): 123.9 (br, ortho-SPhF$_4$CF$_3$), 86.2 (s, para-SPhF$_4$CF$_3$), −199.1 (s, meta-SPhF$_4$CF$_3$). Anal. Calcd for $C_{51}H_{28}F_7FeN_4S$: C, 66.75; H, 3.08; N, 6.11; S, 3.49. Found: C, 66.56; H, 2.96; N, 6.10, S, 3.48. EPR (1/1 CH_2Cl_2/toluene): g_x = 1.945, g_y = 1.96, g_z = 1.975, E/D = 0.03. Yield: 55.0 mg, 82% (starting [Fe(TPP)(OCH$_3$)] mass 51.0 mg).

Synthesis of [Fe(TPP)(SPh(NO$_2$)$_2$-pCH$_3$)]. The thiol used for the preparation of this complex, 2,6-dinitro-*p*-thiocresol (HSPh(NO$_2$)$_2$-*p*CH$_3$), was synthesized as previously reported.[44] UV−vis (toluene): 384, 414, 517, 583, 611, 670, 712 nm. ^{1}H NMR (C_6D_6): 112.35 (s, para-CH$_3$-SPh), 72.2 (br, β-pyrrole H), 68.4 (s, meta-SPh), 12.8 and 11.6 (s, meta-Ph TPP), 9.4 and 5.8 (br, ortho-Ph TPP), 6.4 (s, para-Ph TPP) ppm. EPR (1/1 CH_2Cl_2/toluene): g_x = 1.977, g_y = 1.97, g_z = 1.98, E/D = 0.031. Yield: 54.5 mg, 92% (starting [Fe(TPP)(OCH$_3$)] mass 46.9 mg).

Synthesis of [Fe(TPP)(SPhF$_4$)]. UV−vis (toluene): 412, 513, 575, 605, 671, 715 nm. ^{1}H NMR (C_6D_6): 72.4 (br, β-pyrrole H), 12.7 and 11.8 (s, meta-Ph TPP), 8.8 and 5.9 (br, ortho-Ph TPP), 6.4 (para-Ph, TPP), −93.2 (s, para-SPhF$_4$) ppm. ^{19}F NMR (C_6D_6): 140.1 (br, ortho-SPhF$_4$), −197.8 (s, meta-SPhF$_4$) ppm. EPR (1/1 CH_2Cl_2/toluene): g_x = 1.971, g_y = 1.971, g_z = 1.97, E/D = 0.038. Yield: 57.4 mg, 84% (starting [Fe(TPP)(OCH$_3$)] mass 56.4 mg).

Synthesis of [Fe(TPP)(SPh-3,5-CF$_3$)]. UV−vis (toluene): 408, 513, 575, 668, 710 nm. ^{1}H NMR (C_6D_6): 72.16 (br, β-pyrrole H), 11.9 (s, meta-Ph TPP), 8.8 (br, ortho-Ph TPP), 6.8 (para-Ph TPP), −90.4 (s, ortho-SPh-3,5-CF$_3$), −92.8 (s, para-SPh-3,5-CF$_3$). ^{19}F NMR (C_6D_6): −87.8 (s) ppm. Anal. Calcd for $C_{52}H_{31}F_6FeN_4S$: C, 68.35; H, 3.42; N, 6.13. Found: C, 68.33; H, 3.57; N, 6.24. EPR (1/1 CH_2Cl_2/toluene): g_x = 1.98, g_y = 1.98, g_z = 1.97, E/D = 0.053. Yield: 26.6 mg, 30% (starting [Fe(TPP)(OCH$_3$)] mass 67.7 mg). Note: the complex was observed to be soluble in hexanes to a much higher degree in comparison to any of the other [Fe(TPP)(SPh*)] complexes prepared here. This resulted in a lower yield of the complex due to a greater loss of compound upon recrystallization from CH_2Cl_2/hexanes.

Synthesis of [Fe(TPP)(SPh-pNO$_2$)]. UV−vis (toluene): 407, 514, 575, 670, 710 nm. ^{1}H NMR (C_6D_6): 66.9 (br, β-pyrrole H), 60.2 (s, meta-SPh-*p*NO$_2$), 12.0 (meta-Ph TPP), 8.7 (ortho-Ph TPP), 7.0 (para-Ph TPP), −92.5 (s, ortho-SPh-*p*NO$_2$). Anal. Calcd for $C_{50}H_{32}FeN_5O_2S$: C, 72.99; H, 3.92; N, 8.51. Found: C, 72.42; H, 4.32; N, 8.22. EPR (1/1 CH_2Cl_2/toluene): g_x = 2.1, g_y = 2.15, g_z = 2.2, E/D = 0.035. Yield: 56.8 mg, 78% (starting [Fe(TPP)(OCH$_3$)] mass 67.4 mg).

Synthesis of [Fe(TPP)(SPh-pCF$_3$)]. UV−vis (toluene): 406, 510, 570, 602, 670, 710 nm. ^{1}H NMR (C_6D_6): 62.0 (br, β-pyrrole H), 60.4 (s, meta-SPh-*p*CF$_3$), 11.9 (s, meta-Ph TPP), 9.8 (br, ortho-Ph TPP) 7.6 (s, para-Ph TPP), −94.0(s, ortho-SPh-*p*CF$_3$) ppm. ^{19}F NMR (C_6D_6): 94.8 (s) ppm. EPR (1/1 CH_2Cl_2/toluene): g_x = 1.976, g_y = 1.976, g_z = 1.98, E/D = 0. Yield: 51.9 mg, 64% (starting [Fe(TPP)(OCH$_3$)] mass 67.2 mg).

Synthesis of [Fe(TPP)(SPh)]. This complex was prepared as previously described.[45] UV−vis (toluene): 408, 514, 567, 613, 700 nm. ^{1}H NMR (C_6D_6): 81.4 (br, β-pyrrole H), 63.0 (s, meta-SPh), 11.9 (s, meta-Ph TPP), 8.9 (br, ortho-Ph TPP) 6.6 (s, para-Ph TPP), −94.9 (s, para-SPh) ppm. Yield: 49.0 mg, 56%.

Preparation of the Heme-Thiolate {FeNO}^{6} Complexes. The temperature-sensitive heme-thiolate {FeNO}^{6} samples were prepared for characterization by UV−vis, IR, and rRaman spectroscopy as follows. Approximately 1 equiv of NO(g) was syringed into the headspace of a septum-sealed vial containing a −80 to −90 °C solution of the desired five-coordinate heme-thiolate precursor, mixed, and allowed to react at this temperature for at least 10 min. For IR characterization, the {FeNO}^{6} complexes were prepared in CH_2Cl_2 and then transferred into a solution IR cell using a stainless steel pipet, both of which had been cooled in the cold well along with the sample solution. IR spectra were then continually recorded until all signals of the {FeNO}^{6} complex had diminished.

For rRaman characterization, all samples were prepared in a 1/1 mixture of CH_2Cl_2 and toluene at −80 to −90 °C, transferred to precooled EPR tubes using a precooled stainless steel pipet, capped, and immediately frozen in liquid N_2 upon removal from the glovebox (using a precooled copper block to keep the samples cold in the process).

Density Functional Theory Calculations. All density functional theory (DFT) calculations were performed with the Linux version of the program Gaussian 09.[46] All geometry optimizations and frequency calculations were performed at the BP86/TZVP level, using Becke's 1988 exchange functional[47] and the gradient corrections of Perdew, along with his 1981 local correlation functional P86 (BP86).[48] TZVP is a triple-ζ polarized basis set by Ahlrich and co-workers.[49] Molecular orbitals were obtained from subsequent single-point calculations using the program ORCA at the same level of theory (BP86/TZVP).[50] The heme-thiolate enzyme mimics with two, one, and no hydrogen bonds were generated by starting with the crystallographic coordinates of the heme-thiolate enzyme nNOS (PDB code: 2G6K)[51] and keeping only the coordinates of the Fe−NO protoporphyrin IX complex, Cys415, Trp409, and Gly417. The Cys415 and Trp409 residues were truncated to their side chains, an ethanethiolate and a 3-methylindole, respectively. Gly417 was converted to an *N*-ethylacetamide to better mimic the relevant form in the Cyt P450 active site: i.e., as a backbone amide group. The coordinates of the terminal carbon atoms of the ethanethiolate, the *N*-ethylacetamide, and the protoporphyrin IX propionic acid groups and of the methyl group of 3-methylindole were frozen to conserve their native positions. All other atoms were left unconstrained, and the geometry of the structure was fully optimized. The 3-methylindole and the *N*-ethylacetamide were subsequently removed to generate models with no and one hydrogen bond. The {FeNO}^{6} complexes of these models were then fully optimized preceding frequency calculations. All of these calculations were again performed at the BP86/TZVP level.

For the calculations on the [Fe(P)(SPh)(OOH$_2$)] complex, the O−O bond was frozen at the optimized distance for the hydroperoxo complex [Fe(P)(SPh)(OOH)]$^-$ (1.4664 Å), as optimization of the protonated structure leads to spontaneous O−O bond cleavage, release of H_2O, and generation of a Compound I type species (an [Fe^{IV}═O](Por$^{\bullet+}$)(SPh)] complex). This is in agreement with the mechanism of Cyt P450 monoxygenases. The O−H distances were also fixed (at 0.9857 Å) to prevent proton transfer to the pyrrole nitrogens of the heme. All other parameters where left unconstrained and were allowed to fully optimize.

RESULTS AND ANALYSIS

Hydrogen Bonding versus Electron-Withdrawing Substituents: Finding the Right Thiolate Ligands to Model P450nor. Previous DFT calculations performed by our group predict that the donor strength of the thiolate ligand, as modulated by its hydrogen-bonding network (in Cyt P450 enzymes), is directly reflected in the properties of the Fe−N−O unit in {FeNO}^{6} complexes.[21] In particular, a direct correlation between the thiolate donor strength and the Fe−NO and N−O bond strengths, reflected by the corresponding ν(N−O) and ν(Fe−NO) stretching frequencies, is predicted, but an experimental validation of this claim is missing so far. To better understand Nature's use of hydrogen bonds to control the thiolate donor strength in heme enzymes and to gauge the appropriate type of synthetic thiolate ligand to use that models the {FeNO}^{6} complex of P450nor, we first performed DFT calculations. In particular, since our goal is to use thiophenolate derivatives with electron-withdrawing

DOI: 10.1021/acs.inorgchem.9b00091
Inorg. Chem. XXXX, XXX, XXX−XXX

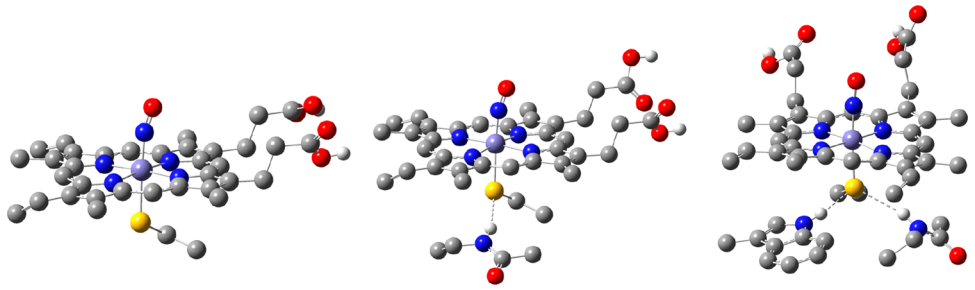

Figure 2. Structures of the DFT enzyme models 0H-B, 1H-B, and 2H-B (from left to right). All three structures were fully optimized using BP86/TZVP. Additional details about these models are provided in the Experimental Section. All non-polar hydrogen atoms have been omitted for clarity.

Table 1. Comparison of Key Parameters of the 0H-B, 1H-B, and 2H-B DFT Models (BP86/TZVP) to Those of the Cyt P450nor {FeNO}^{6} Complex from Crystallographic and Spectroscopic Data

source	complex	ν(NO) (cm^{-1})	Fe−N−O angle (deg)	Fe−N(O) (Å)	N−O (Å)	Fe−S (Å)
DFT	0H-B {FeNO}^{6}	1826	166	1.687	1.163	2.315
DFT	1H-B {FeNO}^{6}	1837	167	1.680	1.161	2.328
DFT	2H-B {FeNO}^{6}	1856	169	1.672	1.159	2.365
enzyme	P450nor {FeNO}^{6}	1851	161	1.63	1.16	2.3
DFT	[Fe(TPP)($SPhF_4CF_3$)(NO)]	1855	169	1.666	1.159	2.374

groups to model the axial thiolate ligand of P450nor, it is a priori not clear what substitution pattern would result in the best agreement with experiment.

In order to accomplish this goal, we used DFT calculations (with BP86/TZVP) on a set of simple Cyt P450 active site models with a different number of H-bonds, as shown in Figure 2, and then optimized the structures of the corresponding {FeNO}^{6} adducts and calculated their vibrational frequencies. The simplest model (0H-B; Figure 2, left) just contains the protoporphyin IX and ethanethiolate as proximal ligand, but no hydrogen bond donors, and provides a baseline with a very strong thiolate donor. In the next step, we added one hydrogen bond, originating from an amide group, similar to those that are provided by the peptide chain in the Cys pocket (1H-B; Figure 2, middle). Note that backbone amides are the most common hydrogen-bond donors to the cysteinate ligand in Cyt P450s and other heme-thiolate enzymes. The final model contains the amide hydrogen bond (in the same relative position), plus an additional hydrogen bond from a tryptophan side chain (2H-B; Figure 2, right), since this amino acid has been reported to be a very strong hydrogen bond donor (inspired by nitric oxide synthase, where this combination of an amide and Trp hydrogen bond to the axial cysteinate ligand is observed).[28] The most important results from these calculations are summarized in Table 1.

By analysis of the DFT results of the heme-thiolate {FeNO}^{6} models with zero, one, and two H-bonds, clear trends can be derived from the calculations. On comparison of the Fe−S bond lengths, it can be seen that 0H-B has the shortest predicted bond length of 2.315 Å, i.e. the strongest Fe−S bond, and that the Fe−S bond decreases in strength with the addition of hydrogen bonds, resulting in Fe−S distances of 2.328 Å for 1H-B and 2.365 Å for 2H-B. This increase in the Fe−S bond distance along this series has significant effects on the calculated Fe−NO and N−O bond distances, which are both predicted to decrease as the number of hydrogen bonds increases. Accordingly, the ν(N−O) and ν(Fe−NO) frequencies increase along the series. The DFT calculations therefore predict a direct correlation of the Fe−NO and N−O bond strengths as a function of the thiolate donor strength, where a stronger Fe−S bond induces weaker Fe−NO and N−O bonds. This trend is evident from Table 1 and has also previously been predicted by DFT for synthetic model systems.[21] The Fe−N−O angle is additionally predicted to become more linear with weaker thiolate donors, going from 166° to 169° for the 0H-B and 2H-B models. A comparison of the calculated ν(N−O) values for these models to the experimentally determined N−O stretching frequency for the {FeNO}^{6} adduct of P450nor shows excellent agreement for the 2H-B model, where the calculated ν(N−O) value of 1856 cm^{-1} is close to the experimental value of 1851 cm^{-1} for P450nor. In summary, the DFT calculations predict that a weaker thiolate donor actually better represents the P450nor {FeNO}^{6} complex.

In terms of generating {FeNO}^{6} model complexes with electron-poor thiophenolate ligands, we then used DFT calculations to predict which thiolate ligand would lead to an {FeNO}^{6} complex with predicted properties that most closely match 2H-B. Our calculations show excellent agreement between 2H-B and the complex with $SR^- = SPhF_4CF_3^-$ (see Scheme 1), as shown in Table 1, which made this complex the first target for our experimental work. The optimized structure of this complex is shown in Figure 3. The calculated properties

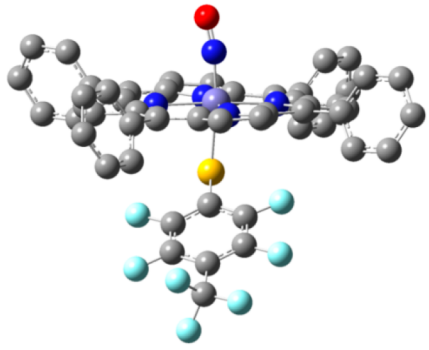

Figure 3. Image of the fully optimized DFT structure of [Fe(TPP)($SPhF_4CF_3$)(NO)] (BP86/TZVP). Hydrogen atoms of the porphyrin have been omitted for clarity.

DOI: 10.1021/acs.inorgchem.9b00091
Inorg. Chem. XXXX, XXX, XXX−XXX

Table 2. Comparison of Key DFT-Calculated Properties (BP86/TZVP) of the Ferric Heme-Nitrosyl Complexes with the Thiophenolate Ligands (SPh^{*-}) Shown in Scheme 1[a]

thiolate	ν(NO) (cm^{-1})	ν(Fe−NO) (cm^{-1})	Fe−N−O angle (deg)	Fe−N(O) (Å)	N−O (Å)	Fe−S (Å)
SPh^-	1825	581	163	1.687	1.163	2.342
SPh-$p$$CF_3^-$	1841	590	166	1.680	1.161	2.346
SPh-$p$$NO_2^-$	1848	589	167	1.676(6)	1.159(7)	2.353
SPh-3,5-CF_3^-	1850	590	168	1.676(8)	1.159(6)	2.350
$SPhF_4^-$	1850	592	168	1.675	1.159(7)	2.360
$SPhF_4CF_3^-$	1860	598	170	1.670	1.158(3)	2.370
SPh$(NO_2)_2$-$p$$CH_3^-$	1863	600	173	1.665	1.158(5)	2.386

[a]The porphine dianion (P^{2-}) was used for all calculations shown here.

for this complex closely match a number of the key parameters of the 2H-B model, including the Fe−N−O angle (169°), the N−O bond distance (1.159 Å), and the very similar calculated ν(N−O) (1856 vs 1855 cm^{-1}). The advantage of using thiophenolates as the basis to develop a series of $\{FeNO\}^6$ complexes with thiolates of different donor strength is the fact that many thiophenols with a broad spectrum of electron-donating and -withdrawing substituents are commercially available. It is surprising though that the very "electron poor" thiophenolate $SPhF_4CF_3^-$ is predicted to give a $\{FeNO\}^6$ complex that closely matches the electronic properties of the NO adduct of ferric P450nor. Table 2 gives the DFT-calculated geometric and vibrational properties for the complete series of thiolate-coordinated model complexes investigated here, using the thiophenolate ligands shown in Scheme 1.

Having these predictions from DFT calculations in hand, we then set off to test our hypothesis by first synthesizing the five-coordinate heme-thiolate complex [Fe(TPP)(SPh_4CF_3)] and then reacting this compound with NO(g) at −80 °C to form the corresponding $\{FeNO\}^6$ complex.

Synthesis of Five-Coordinate Ferric Heme-Thiolate Model Complexes. To prepare five-coordinate ferric heme-thiolate complexes of the type [Fe(TPP)(SPh^*)] (TPP^{2-} = tetraphenylporphyrin dianion; SPh^{*-} = thiophenolate derivative) directly from the free thiols in high purity, we have further developed a synthetic method that starts from the ferric methoxide complex, where the methoxide ligand acts as an internal, strong base. For example, the synthesis of [Fe(TPP)(SPh_4CF_3)] was accomplished by reacting [Fe(TPP)(OCH_3)] with a slight excess of 4-trifluoromethyl-2,3,5,6-tetrafluorothiophenol ($HSPhF_4CF_3$), in which an acid−base ligand exchange occurs that generates the desired five-coordinate heme-thiolate complex and methanol as the products, according to the equation:

$$[Fe(TPP)(OCH_3)] + HSPhF_4CF_3 \rightarrow [Fe(TPP)(SPh_4CF_3)] + CH_3OH$$

This type of acid/base thiol/methoxide ligand exchange reaction has previously been used by Tonzetich and co-workers for the synthesis of pure ferric heme-silanethiolate complexes[52] and for the preparation of [Ru(TTP)(NO)(SR)] by reaction of [Ru(TTP)(NO)(OMe)] with the corresponding thiol.[53] This reaction is extremely fast, and a characteristic color change from dark green to dark red-brown is observed immediately after the thiol is added to a solution of the ferric TPP methoxide complex. This is further documented in Figure 4: here, the methoxide complex shows the Soret band at 416 nm, and after addition of $HSPhF_4CF_3$, a split Soret band is

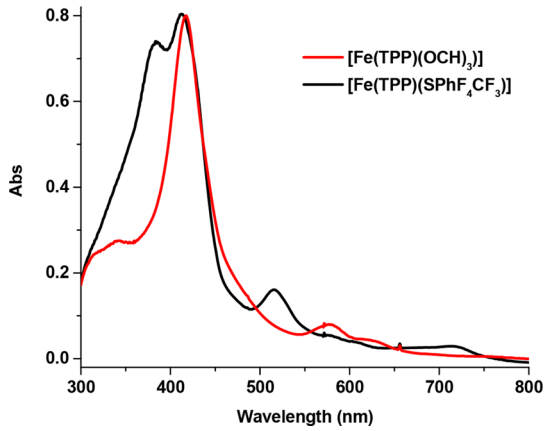

Figure 4. UV−vis spectra of [Fe(TPP)(OCH_3)] (black) and [Fe(TPP)($SPhF_4CF_3$)] (red), in CH_2Cl_2 at room temperature.

observed by UV−vis spectroscopy with λ_{max} at 413 and 384 nm. In the Q-band region, a unique pattern with bands at 515, 581, 608, 675, and 716 nm is observed, which is characteristic for high-spin ferric [Fe(TPP)(SR)] type complexes. Any excess thiol left after the reaction using this method can then be easily removed by evaporation of the solvent under reduced pressure, followed by collecting solid heme-thiolate complex on a frit by vacuum filtration and washing the solid with methanol. After drying of the obtained complex [Fe(TPP)-($SPhF_4CF_3$)] under vacuum to remove residual solvent, the complex was then further characterized by ^1H and ^{19}F NMR spectroscopy to ensure purity (see Figures S1 and S2). Characteristic paramagnetic shifts in the ^1H NMR spectra of [Fe(TPP)($SPhF_4CF_3$)] are observed, which demonstrate that this is a high-spin (S = 5/2) ferric complex. In particular, the β-pyrrole protons of the heme are shifted to 71.8 ppm. The ^{19}F NMR spectra exhibit three paramagnetically shifted signals for the three unique fluorine environments of the bound $SPhF_4CF_3^-$ ligand (Figure S2). All other five-coordinate ferric heme-thiolate complexes were prepared in an analogous way. By comparison, the paramagnetic signals not belonging to the high-spin ferric $[Fe(TPP)]^+$ unit can be identified, and in this way, the paramagnetically shifted ^1H and ^{19}F signals of the bound thiophenolate ligands can be assigned in a systematic way (see Figure 5). Assignments for all ^1H chemical shifts are summarized in Table 3.

Additionally, all of the precursor complexes were characterized by EPR spectroscopy. The EPR spectrum of [Fe-(TPP)($SPhF_4CF_3$)] (Figure S3) displays a rhombic S = 5/2 signal with effective g values of 6.6, 5.1, and 1.95, again confirming that the complex is a five-coordinate high-spin

DOI: 10.1021/acs.inorgchem.9b00091
Inorg. Chem. XXXX, XXX, XXX−XXX

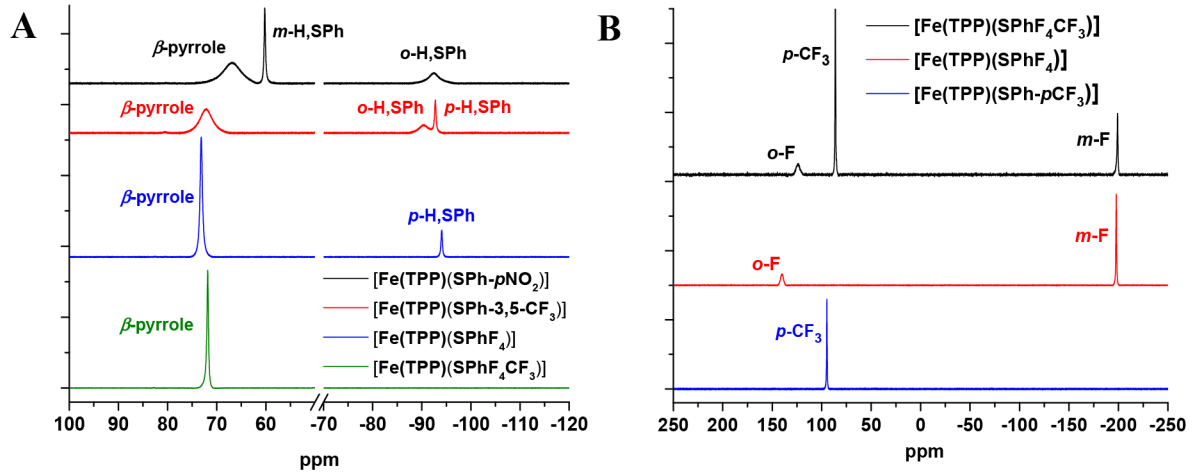

Figure 5. (A) Overlay of ^{1}H NMR spectra of selected high-spin ferric [Fe(TPP)(SPh*)] complexes, indicating the assignments of the ortho (*o*-), meta (*m*-), and para (*p*-) phenyl protons of the bound thiophenolate ligands. (B) Overlay of the ^{19}F NMR spectra of [Fe(TPP)($SPhF_4CF_3$)], [Fe(TPP)($SPhF_4$)], and [Fe(TPP)(SPh-*p*CF_3)], showing the signals of the bound thiophenolate ligands.

Table 3. Assignments of the ^{1}H NMR Chemical Shifts of the Seven Ferric Heme-Thiolate Complexes Shown in Scheme 1, Recorded in C_6D_6 at Room Temperature

complex	β-pyrrole H	m-Ph, TPP	o-Ph, TPP	p-Ph, TPP	m-Ph, SPh	o-Ph, SPh	p-Ph, SPh
[Fe(TPP)($SPhF_4CF_3$)]	71.8	13.2, 11.9	9.0, 5.8	6.4			
[Fe(TPP)(SPh(NO_2)$_2$-*p*CH_3)]	72.2	12.8, 11.6	9.4, 5.8	6.4	68.4		
[Fe(TPP)($SPhF_4$)]	72.4	12.7, 11.8	8.8, 5.9	6.4			−93.2
[Fe(TPP)(SPh-3,5-CF_3)]	72.2	11.9	8.8	6.8		−90.4	−92.8
[Fe(TPP)(SPh-*p*NO_2)]	66.9	12.0	8.7	7.0	60.2	−92.5	
[Fe(TPP)(SPh-*p*CF_3)]	81.3	11.9	9.8	7.6	60.4	−94.0	
[Fe(TPP)(SPh)]	81.4	11.9	8.9	6.6	63.0	N/D	−94.9

Scheme 2. Potential Reaction Pathways of Ferric Heme-Thiolate Model Complexes with NO, Which Ultimately Generate Ferrous Heme-Nitrosyl ({FeNO}^{7}) Decomposition Products

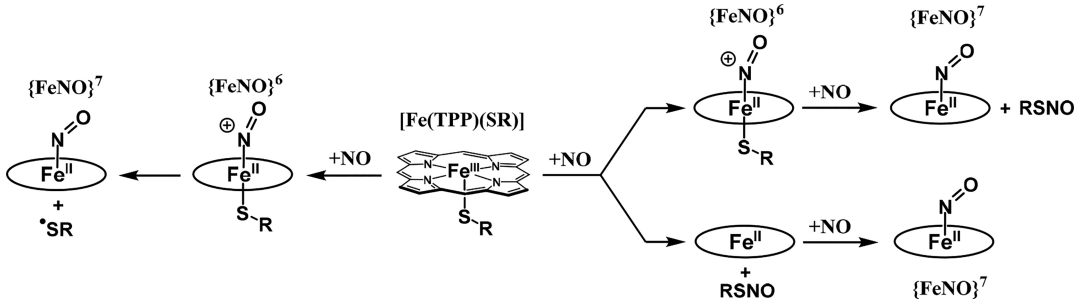

heme-thiolate complex. A simulation of the EPR data yields an *E*/*D* value of 0.03, as shown in Figure S3.

As mentioned above, all other [Fe(TPP)(SPh*)] complexes with the thiolate ligands shown in Scheme 1 were synthesized using the same method. Figures S10−S30 in the Supporting Information show the basic spectroscopic characterization of all of these complexes, using UV−vis absorption, NMR, EPR, and vibrational spectroscopy. It is noted that this thiol/methoxide ligand exchange method works best when more acidic thiols are used, such as those used here. On the other hand, the reaction of [Fe(TPP)(OCH_3)] with the more basic thiol, *p*-thiocresol (HSPh-*p*CH_3), leads to complete reduction to the ferrous [Fe(TPP)] complex, as is evident from UV−vis spectroscopy (data not shown). Reaction of [Fe(TPP)(OCH_3)] with HSPh leads to formation of a mixture of [Fe(TPP)(SPh)] and [Fe(TPP)], as previously observed by Tonzetich and co-workers.[52] For this reason, [Fe(TPP)(SPh)] was prepared by an alternative method as described previously.[45]

Reaction of Ferric Heme-Thiolate Model Complexes with Nitric Oxide. Whereas {FeNO}^{6} complexes with thiolate coordination are relatively stable in protein active site environments, the generation of the corresponding model complexes has remained highly elusive. One challenge in generating ferric heme-nitrosyl complexes in general is their decomposition into the corresponding five-coordinate, ferrous heme-nitrosyl complexes [Fe(Porph)(NO)] (Porph^{2-} = general porphyrin dianion), or {FeNO}^{7} species in the Enemark-Feltham notation, in the presence of excess NO and various nucleophiles, including alcohols, water, amines, and thiols. This is due to a process known as "reductive nitrosylation".[54−56] Simple [Fe(Porph)(SR)(NO)] model complexes suffer from additional instability in comparison to {FeNO}^{6} complexes coordinated by N-donor ligands, due to

DOI: 10.1021/acs.inorgchem.9b00091
Inorg. Chem. XXXX, XXX, XXX−XXX

the instability of the thiolate ligand in the presence of NO. Here, NO can directly nitrosylate the coordinated thiolate ligand, leading to decomposition. Finally, homolytic cleavage of the Fe−S bond after NO coordination is also possible, depending on the nature of the thiolate.[44] Ultimately, both of these latter pathways again lead to generation of the corresponding ferrous [Fe(Porph)(NO)] complex. These potential decomposition pathways are summarized in Scheme 2.

Correspondingly, whereas many (>8) {FeNO}^{6} complexes with bound axial imidazole or other neutral N-heterocyclic ligands have been generated and structurally characterized,[24,36,57−59] there is only one reported crystal structure of a thiolate-coordinated {FeNO}^{6} complex, [Fe(OEP)(SR-H_2)(NO)] (SR-H_2^- = S-2,6-$(CF_3CONH)_2C_6H_3$; OEP^{2-} = octaethylporphyrin dianion), available to this date.[30] Here, the thiolate ligand utilizes two strong amide hydrogen bonds for stabilization, and this compound is in fact able to reversibly bind NO at low temperatures.[31] Still, the crystal structure of this complex could only be obtained by diffusion of NO gas into the crystal lattice of the five-coordinate heme-thiolate precursor, again emphasizing the stability challenges for generating [Fe(Porph)(SR)(NO)] model complexes.

As indicated above, previous work in our group has found that reaction of ferric Fe(TPP) complexes with bound thiophenolates, such as [Fe(TPP)(SPh)], with NO at room temperature or at −40 °C results in direct conversion to the ferrous heme-nitrosyl complex [Fe(TPP)(NO)].[44] Starting from these results, we speculated that application of electron-poor thiophenolates in combination with improved experimental conditions (especially conducting experiments at −80 °C) might allow us to finally observe and characterize the corresponding {FeNO}^{6} complexes. Since the DFT results (see above) indicated that [Fe(TPP)($SPhF_4CF_3$)(NO)] is a good electronic−structural model for the {FeNO}^{6} adduct of P450nor, we first investigated the reaction of the corresponding ferric precursor with NO. Figure 6 shows the spectral changes observed by UV−vis spectroscopy when [Fe(TPP)-($SPhF_4CF_3$)] is reacted with NO gas at −80 °C, monitored in situ using a Hellma immersion probe. Addition of NO causes

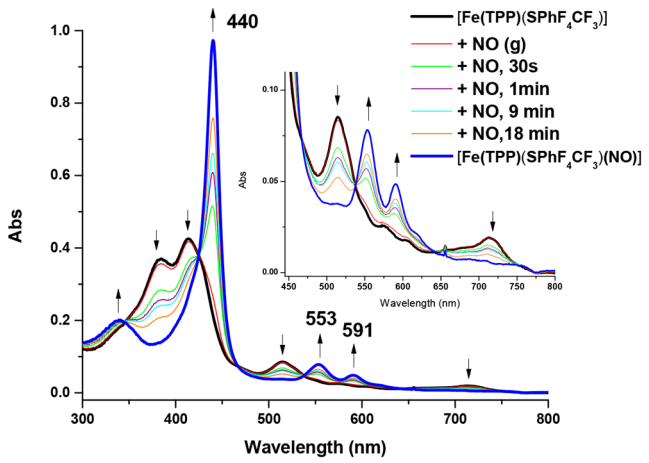

Figure 6. UV−vis spectra monitoring the reaction between [Fe(TPP)($SPhF_4CF_3$)] (black) and NO, upon addition of NO(g) to a solution of the complex at −80 °C in toluene. Insert: expanded view of the Q-band region between 450 and 800 nm. Arrows indicate the intensity changes of the absorption features over time.

the disappearance of the Soret band at 413 nm of the precursor and the appearance of a new, intense Soret feature at 440 nm and two new Q bands at 553 and 591 nm. Additionally, isosbestic points are observed at ∼345, 425, 465, 537, and 645 nm, indicating that a simple one-step reaction between NO and [Fe(TPP)($SPhF_4CF_3$)] takes place. This new species is stable at −80 °C, and no signs of decomposition into the {FeNO}^{7} complex are observed for ∼2 h when the solution is kept at this temperature (we did not monitor the solution past 2 h, and so it is not clear at what point decomposition would occur). Upon removal of the solution from the cold well and warming it to room temperature, signals for the {FeNO}^{6} complex start to slightly decrease when the solution temperature reaches approximately −60 °C. Further warming then leads to significant decomposition to the five-coordinate {FeNO}^{7} complex [Fe(TPP)(NO)] (Figure S4). By −10 °C the solution has almost fully converted to the {FeNO}^{7} complex.

In summary, reaction of [Fe(TPP)($SPhF_4CF_3$)] with NO(g) at −80 °C results in a new stable species, until the solution is warmed, suggesting that this new species is the corresponding ferric heme-nitrosyl complex [Fe(TPP)-($SPhF_4CF_3$)(NO)]. In support of this idea, the UV−vis spectrum observed for this complex matches quite well with those reported for heme-thiolate {FeNO}^{6} adducts in enzymes. For example, the ferric-nitrosyl adduct of nNOS is reported to have a Soret band at 440 nm and two Q bands at 549 and 580 nm, with the same intensity ordering as observed in our new species (where these features are located at 553 and 591 nm).[60] Next, to confirm the exact nature of the reaction product between [Fe(TPP)($SPhF_4CF_3$)] and NO at −80 °C, we performed solution IR and resonance Raman (rRaman) spectroscopy to measure the ν(N−O) and ν(Fe−NO) vibrations, respectively.

Solution IR characterization of the new species observed in the UV−vis experiments was conducted by addition of ∼1 equiv of NO(g) to a −80 to −90 °C solution of [Fe(TPP)($SPhF_4CF_3$)] in CH_2Cl_2, stirring of the solution for 10 min, and then quickly transferring the reaction mixture to a precooled solution IR cell, followed by immediate collection of the IR spectra as the solution warmed up. Upon doing so, a large signal at 1867 cm^{-1} was observed in the first scan (Figure 7). Additional spectra of the solution were continually recorded as the solution gradually warmed up inside the spectrometer, until the signal at 1867 cm^{-1} had completely disappeared. As this signal decreased in intensity, a new signal was observed at 1675 cm^{-1} that proportionally increased in intensity. Repeating this experiment with isotopically labeled $^{15}N^{18}O$(g) shifted the observed band at 1867 to 1792 cm^{-1}. Similar to the experiment with natural abundance isotopes (n.a.i.) NO, the signal at 1792 cm^{-1} decreased in intensity as the solution warmed up, with the appearance of a new band at 1607 cm^{-1} (Figure 8). The isotope sensitivity of the band at 1867 cm^{-1} confirms the assignment of this feature to the N−O stretch of the new six-coordinate {FeNO}^{6} heme-thiolate complex [Fe(TPP)-($SPhF_4CF_3$)(NO)], observed in the UV−vis experiments at −80 °C. The appearance of the 1675 cm^{-1} feature (1607 cm^{-1} with $^{15}N^{18}O$) further confirms that [Fe(TPP)(NO)] is formed as the decomposition product of [Fe(TPP)($SPhF_4CF_3$)(NO)], as the reaction mixture warms up. An overlay of the first scan of the IR experiment with n.a.i. NO and $^{15}N^{18}O$ is shown in Figure S5.

DOI: 10.1021/acs.inorgchem.9b00091
Inorg. Chem. XXXX, XXX, XXX−XXX

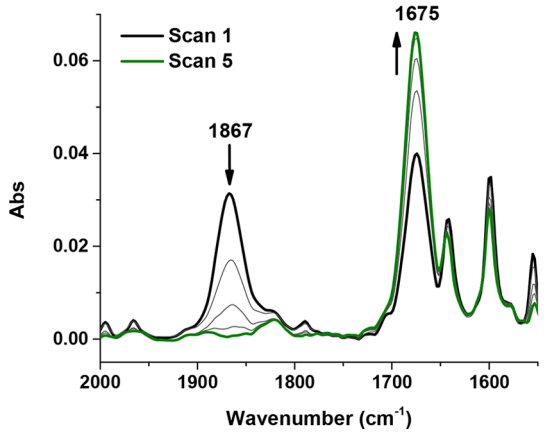

Figure 7. Solution IR spectra of [Fe(TPP)(SPhF$_4$CF$_3$)(NO)] recorded in CH_2Cl_2. Scan 1 (black) is the first IR spectrum recorded upon injection of the solution of [Fe(TPP)(SPhF$_4$CF$_3$)(NO)] into the solution IR cell at −80 °C. Additional scans are shown in gray as the solution warmed up to room temperature. By scan 5 (green), the solution has been fully converted to the five-coordinate ferrous heme-nitrosyl complex [Fe(TPP)(NO)].

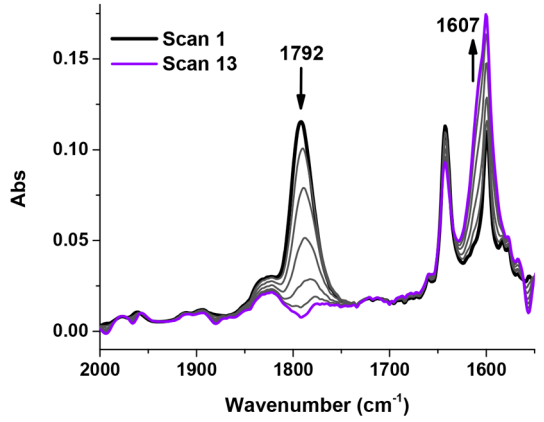

Figure 8. Solution IR spectra of [Fe(TPP)(SPhF$_4$CF$_3$)(^{15}N^{18}O)] recorded in CH_2Cl_2. Scan 1 (black) is the first IR spectrum recorded upon injection of the solution of [Fe(TPP)(SPhF$_4$CF$_3$)(^{15}N^{18}O)] into the solution IR cell at −80 °C. Additional scans are shown in gray as the solution warmed up to room temperature. By scan 13 (purple), the solution has been fully converted to the five-coordinate ferrous heme-nitrosyl complex [Fe(TPP)(^{15}N^{18}O)].

Next, [Fe(TPP)(SPhF$_4$CF$_3$)(NO)] was characterized by rRaman spectroscopy at 77 K to determine the Fe−NO stretch of this complex, using 458 nm laser excitation. This laser wavelength was chosen due to its proximity in energy to the Soret band of the complex at 440 nm. An overlay of the spectra in the low-energy region obtained for [Fe(TPP)(SPhF$_4$CF$_3$)(NO)] and the corresponding ^{15}N^{18}O complex is shown in Figure 9. Here, an isotope-sensitive band is observed at 543 cm^{-1} that shifts to 530 cm^{-1} in the ^{15}N^{18}O complex (difference 13 cm^{-1}), allowing us to directly assign this feature to the Fe−NO stretch of [Fe(TPP)(SPhF$_4$CF$_3$)(NO)]. The complete rRaman spectra of the n.a.i. and isotopically labeled NO complexes, of the 1/1 CH_2Cl_2/toluene solvent mixture, and of the five-coordinate ferric heme-thiolate precursor are provided in Figures S7−S9 in the Supporting Information.

Synthesis and Testing of Additional Ferric Heme-Thiolate Complexes. The successful generation of [Fe(TPP)(SPFh$_4$CF$_3$)(NO)] represents the first characterization

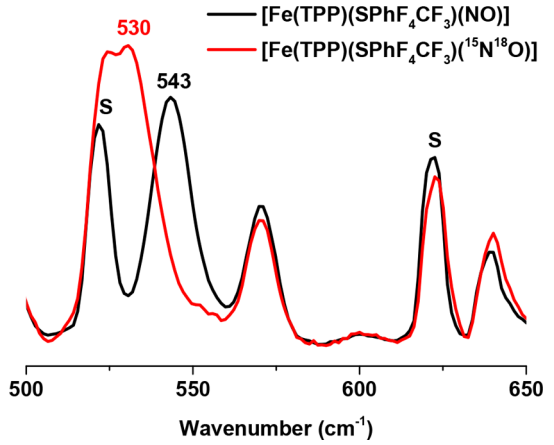

Figure 9. Overlay of the low-energy region of the resonance Raman spectra (458 nm excitation) of [Fe(TPP)(SPhF$_4$CF$_3$)(NO)] and [Fe(TPP)(SPhF$_4$CF$_3$)(^{15}N^{18}O)], each one prepared in a 1/1 CH_2Cl_2/toluene mixture. Data were collected at 77 K. The solvent bands of toluene are marked with S (see Figure S8 for the full spectrum of the solvent mixture).

of a heme-thiolate {FeNO}^{6} complex with TPP^{2-} as the porphyrin coligand to date. To further vary the electronic nature of the thiolate ligand in heme-thiolate {FeNO}^{6} model complexes, we then applied the same method used to generate [Fe(TPP)(SPFh$_4$CF$_3$)(NO)] to the other five-coordinate ferric heme-thiolate precursors with the thiolate ligands shown in Scheme 1. First, the additional thiolate complexes were synthesized by reaction of the corresponding thiols 2,3,5,6-tetrafluorobenzenethiol (HSPhF$_4$), 4-(trifluoromethyl)-thiophenol (HSPh-pCF$_3$), 4-nitrothiophenol (HSPh-pNO$_2$), 2,6-dinitrothiocresol (HSPh(NO$_2$)$_2$-pCH$_3$), and 3,5-bis-(trifluoromethyl)thiophenol (HSPh-3,5-CF$_3$) with [Fe(TPP)-(OCH$_3$)] as described above. After successful synthesis and characterization (Figures S10−S28), the five-coordinate heme-thiolate complexes were then individually reacted with NO(g) at −80 °C while the reaction was monitored with in situ UV−vis spectroscopy. For [Fe(TPP)(SPh(NO$_2$)$_2$-pCH$_3$)] and [Fe(TPP)(SPhF$_4$)], stable new species were observed, similar to the results for [Fe(TPP)(SPhF$_4$CF$_3$)], with intense Soret bands close to 440 nm and two new Q-bands in the 550 and 590 nm region (Figures S31 and S34). Warming the solutions to room temperature resulted in decomposition of these new species, generating [Fe(TPP)(NO)]. The {FeNO}^{6} adducts were then further characterized by IR and rRaman spectroscopy to determine their N−O and Fe−NO stretching frequencies. These were observed at 1863 and 547 cm^{-1} for [Fe(TPP)(SPh(NO$_2$)$_2$-pCH$_3$)(NO)] and 1860 and 538 cm^{-1} for [Fe(TPP)(SPhF$_4$)(NO)] (Figures S32 and S33 and Figures S35 and S36, respectively).

Encouraged by these positive results with the very electron poor thiolate ligands SPFh$_4$CF$_3^-$, SPhF$_4^-$, and SPh(NO$_2$)$_2$-pCH$_3^-$, we then tested whether the {FeNO}^{6} adduct could also be obtained for the complex [Fe(TPP)(SPh-pCF$_3$)], which contains a distinctively more electron rich (and hence more donating) thiolate. Upon reaction of [Fe(TPP)(SPh-pCF$_3$)] with low equivalents of NO(g) at −80 °C, a new species is observed to form with UV−vis spectral features similar to those of the other three {FeNO}^{6} complexes, with a new Soret band at 440 nm and two new prominent Q-bands at 556 and 597 nm (Figure 10A). After addition of a total of 1 equiv of NO(g), this new species, [Fe(TPP)(SPh-pCF$_3$)-

DOI: 10.1021/acs.inorgchem.9b00091
Inorg. Chem. XXXX, XXX, XXX−XXX

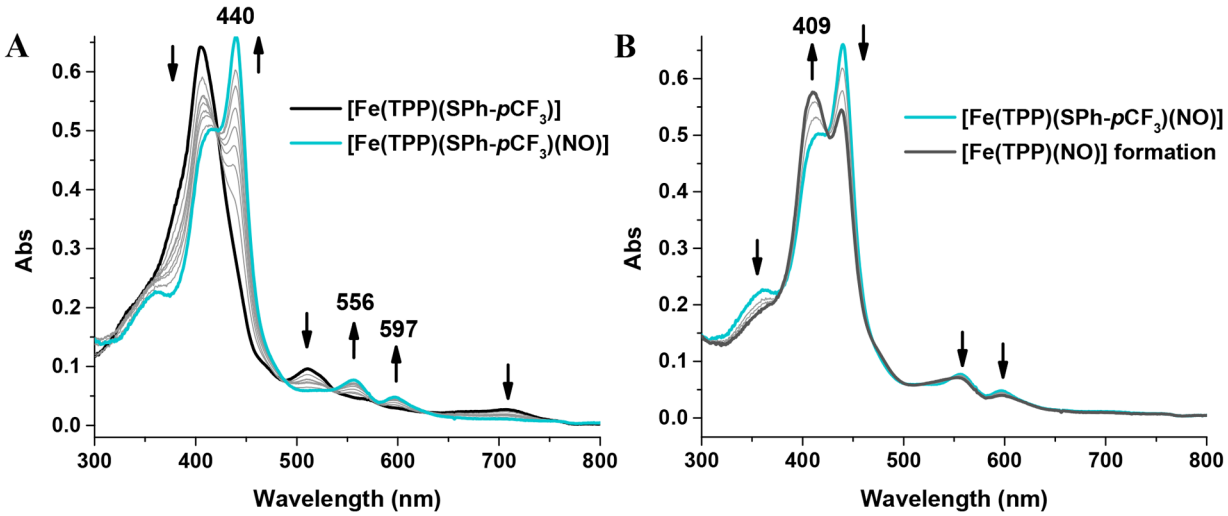

Figure 10. UV−vis spectra monitoring the reaction between [Fe(TPP)(SPh-pCF$_3$)] (black) and NO(g) at −80 °C in toluene: (A) initial spectral changes observed for the reaction with ∼1 equiv of NO(g) added to the solution; (B) changes observed upon addition of another ∼0.25 equiv of NO.

(NO)], is observed to form in approximately 40−50% yield (by comparison to the intensity of the Soret band of [Fe(TPP)(SPhF$_4$CF$_3$)(NO)]; see Figure 6). After no further changes were observed in the spectra, an additional ∼0.25 equiv of NO(g) was added to the solution, resulting in a brief, initial increase in the Soret band intensity at 440 nm, followed by a subsequent intensity drop and formation of a new band at ∼409 nm, representing the generation of [Fe(TPP)(NO)] (Figure 10B). On the basis of these results, [Fe(TPP)(SPh-pCF$_3$)] represents the borderline in terms of thiolate donor strength that still allows for the formation of the {FeNO}^{6} adduct at −80 °C. This incomplete conversion to [Fe(TPP)-(SPh-pCF$_3$)(NO)] in the UV−vis experiments can be rationalized to occur via a direct attack of NO at the bound thiolate ligand in some of the [Fe(TPP)(SPh-pCF$_3$)] precursor, generating the nitrosothiol and [Fe(TPP)], which subsequently binds another NO molecule. Hence, 2 equiv of NO are consumed in this process without generating any [Fe(TPP)(SPh-pCF$_3$)(NO)], lowering the amount of NO gas in solution. Upon the addition of more NO, the remaining [Fe(TPP)(SPh-pCF$_3$)] can be transformed into the corresponding {FeNO}^{6} complex. Once all of the precursor has been consumed, excess NO in solution might then be able to attack the thiolate ligand in the product complex, [Fe(TPP)-(SPh-pCF$_3$)(NO)] (top right in Scheme 2). At this point, more [Fe(TPP)(NO)] is generated and becomes visible in the UV−vis spectra. Regardless of this, since a significant amount of [Fe(TPP)(SPh-pCF$_3$)(NO)] is still formed at −80 °C (especially with substoichiometric amounts of NO), we were able to characterize this compound by solution IR and rRaman spectroscopy, showing its N−O and Fe−NO stretches at 1847 and 532 cm^{-1}, respectively (Figures S37−S39). On the basis of these experimental results, it can be concluded that [Fe(TPP)-(SPh-pCF$_3$)(NO)] actually shows the best agreement with the ν(N−O) and ν(Fe−NO) vibrational energies of the P450nor {FeNO}^{6} adduct (1851 and 530 cm^{-1}), and hence, this complex is a very good electronic−structural model for the NO adduct of P450nor. Note that this is at odds with the DFT results (see above), which predict that [Fe(TPP)(SPhF$_4$CF$_3$)-(NO)] should be a better electronic model for the enzyme's ferric NO complex. On the basis of the experimental results, [Fe(TPP)(SPhF$_4$CF$_3$)(NO)] is actually a better electronic−structural model for the NO adducts of the heme-thiolate enzymes CPO and NOS (see Table 4).

Table 4. Comparison of ν(N−O) and ν(Fe−NO) Stretching Frequencies of Synthetic and Enzymatic Heme-Thiolate {FeNO}^{6} Complexes[a]

{FeNO}^{6} complex	ν(N−O)	ν(Fe−NO)	ref
[Fe(TPP)(SPhF$_4$CF$_3$)(NO)]	1867	543	TW
[Fe(TPP)(SPh(NO$_2$)$_2$-pCH$_3$)(NO)]	1863	547	TW
[Fe(TPP)(SPhF$_4$)(NO)]	1860	538	TW
[Fe(TPP)(SPh-3,5-CF$_3$)(NO)]	1855	537	TW
[Fe(TPP)(SPh-pNO$_2$)(NO)]	1852	535	TW
[Fe(TPP)(SPh-pCF$_3$)(NO)]	1847	532	TW
iNOSoxy (+H4B)	1872	541	29, 68
iNOSoxy	1870	537	29, 68
CPO	1868	538	27
P450nor (proto)	1853	530	69
P450nor (meso)	1852	532	69
P450nor (deutero)	1851	533	69
P450nor (WT)	1851	530	25
Cyt P450cam	1806	528	25, 26

[a]TW = this work.

Finally, the complexes [Fe(TPP)(SPh-pNO$_2$)(NO)] and [Fe(TPP)(SPh-3,5-CF$_3$)(NO)] with two additional thiolates of intermittent donor strength were also prepared and spectroscopically characterized (Figures S40−S45). In the case of the p-nitro-substituted thiophenolate ligand, the reaction with NO would again not go to completion, but enough of the NO adduct formed for full vibrational characterization.

We had previously attempted to generate an {FeNO}^{6} complex with [Fe(TPP)(SPh)] at −40 °C, but conversion to [Fe(TPP)(NO)] was solely observed under those conditions.[44] We therefore retested the reaction of [Fe(TPP)(SPh)] with NO(g) at −80 °C. As shown in Figure S46, upon addition of ∼1 equiv of NO a small amount of a new species is observed

DOI: 10.1021/acs.inorgchem.9b00091
Inorg. Chem. XXXX, XXX, XXX−XXX

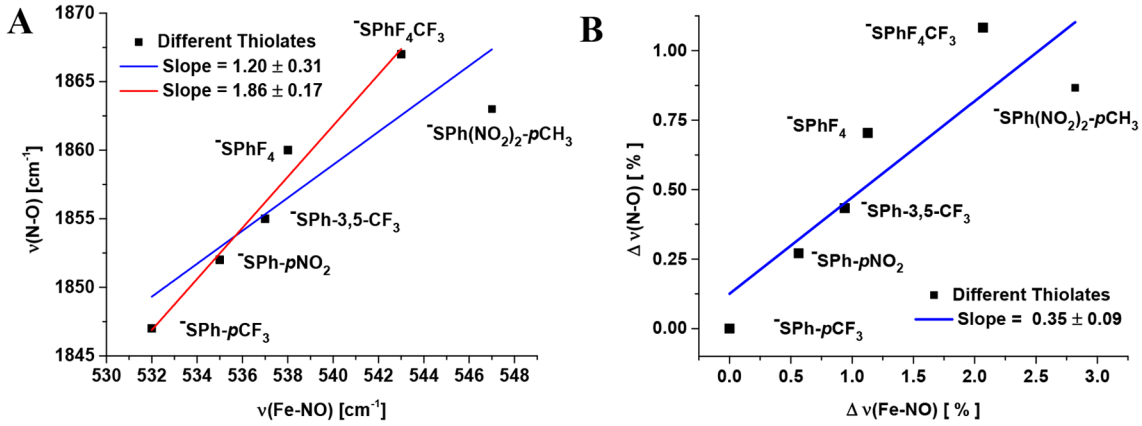

Figure 11. (A) Correlation plot comparing the experimentally determined ν(Fe−NO) and ν(N−O) stretching frequencies from rRaman and IR spectroscopy, respectively. The red line is the best linear fit of the data of the {FeNO}^{6} complexes with the four fluoro-containing thiolates and SPh-pNO$_2^-$. The blue line is the linear fit for all six complexes (including the SPh(NO$_2$)$_2$-pCH$_3^-$ compound). (B) The same plot, but now shown as a relative change of the Fe−NO and N−O stretching frequencies, setting the vibrational frequencies of [Fe(TPP)(SPh-pCF$_3$)(NO)] to zero.

under these conditions with a Soret band at 439 nm and Q-bands at 558 and 598 nm, indicating formation of a small amount of the {FeNO}^{6} adduct. However, these signals quickly decrease in intensity, and conversion of the spectrum to that of the {FeNO}^{7} complex [Fe(TPP)(NO)] is observed, even without a subsequent NO addition. Importantly, these results indicate that with more electron-rich thiolates such as SPh$^-$, either a direct attack of NO at the thiolate ligand to form PhS-NO and the ferrous porphyrin (which subsequently binds NO and forms [Fe(TPP)(NO)]) is preferred over the reaction of NO with the open coordination site of the ferric heme, or homolytic cleavage of the Fe−SPh bond occurs upon generation of the {FeNO}^{6} complex. This attack of NO at the Fe−S bond in heme-thiolate model systems has previously been reported,[61] and S-nitrosylation has also been observed crystallographically in the heme-thiolate type nitrophorins.[62] With respect to Scheme 2, this indicates that the electron richness of the thiolate is one factor that determines whether the reaction proceeds to the left or right of the scheme and that [Fe(TPP)(SPh-pCF$_3$)] and [Fe(TPP)(SPh-pNO$_2$)] are in fact right on the borderline, as pointed out above. To explore whether temperature could be a factor in improving the formation of [Fe(TPP)(SPh)(NO)] or the stability of [Fe(TPP)(SPh-pCF$_3$)(NO)], we then repeated the reactions of [Fe(TPP)(SPh)] and [Fe(TPP)(SPh-pCF$_3$)] with NO(g) at −125 °C in 2-methyltetrahydrofuran (2-MeTHF). However, these experiments resulted in direct conversion of [Fe(TPP)(SPh)] to the corresponding {FeNO}^{7} complex [Fe(TPP)(NO)] (data not shown). In the case of [Fe(TPP)(SPh-pCF$_3$)], even less of the {FeNO}^{6} complex accumulated before decomposition to [Fe(TPP)(NO)] occurred (Figure S47). On the basis of the UV−vis spectra, we speculate that in 2-MeTHF the corresponding six-coordinate complexes [Fe(TPP)(SPh*)(2-MeTHF)] form, which actually inhibits NO coordination to the Fe center and instead promotes attack at the thiolate. Hence, the decrease in temperature likely offers no additional benefit toward the successful generation of [Fe(TPP)(SPh*)(NO)] type complexes in 2-MeTHF.

Correlation between the ν(N−O) and ν(Fe−NO) Stretching Frequencies. Figure 11A compares the values of the ν(N−O) and ν(Fe−NO) stretching frequencies (Table 4) for our series of thiolate-coordinated {FeNO}^{6} complexes visually, in the form of a correlation plot. These results *demonstrate experimentally that the Fe−NO and N−O bond strengths (and correspondingly, the stretching frequencies) are indeed directly correlated to the thiolate donor strength*. For example, as the thiolate donicity *decreases* (going from left to right in Figure 11A), both the N−O and Fe−NO stretching frequencies continually *increase*. Correspondingly, the complex with the strongest thiolate donor, [Fe(TPP)(SPh-pCF$_3$)(NO)], has the lowest observed ν(N−O) and ν(Fe−NO) stretching frequencies in the series. Figure 11A also shows two different linear fits of the data. When only the fluorine-substituted thiolates and SPh-pNO$_2^-$ are considered, a perfect correlation of the vibrational data is observed, as shown by the red line in Figure 11A. When the dinitro-substituted compound is included in the fit, the blue correlation line in Figure 11A is obtained. The deviation of the vibrational properties of the dinitro-thiophenolate complex from the correlation line is likely caused by effects other than those purely electronic in nature. We speculate that the bulky *o*-dinitro substituents also impart steric effects on the resulting NO complex, causing the observed deviations. These differences aside, *the correlation plot provides experimental evidence, for the first time, that the thiolate ligand is in fact directly responsible for modulating the N−O and Fe−NO bond strengths in heme-thiolate {FeNO}^{6} complexes*.

This is a very important finding, as the direct correlation between the Fe−NO and N−O bond strengths now proven experimentally provides direct evidence for the electronic mechanism by which the thiolate donor is able to exert this effect on the Fe−N−O unit. This finding is in contrast to the inverse correlation observed for ferrous heme-carbonyl complexes.[63] In this case, variation of the trans ligand to CO changes the Fe−CO π back-bond. A weakening of the π back-bond, for example, would decrease the Fe−CO stretch (because of the weaker metal−CO bond) and, at the same time, increase the C−O stretch (due to the decrease in the occupation of the CO(π^*) orbitals). As established by Spiro, such an inverse correlation is therefore a hallmark of a variation in metal−ligand π back-bonding.[63] Previous work has shown that heme {FeNO}^{6} complexes have Fe^{II}−NO$^+$ type electronic structures, irrespective of the trans ligand to NO, and that in this case the Fe^{II}−NO$^+$ interaction is dominated by π back-bonding (as in the case of the isoelectronic Fe^{II}−CO complexes). It is therefore very surprising that the variation

DOI: 10.1021/acs.inorgchem.9b00091
Inorg. Chem. XXXX, XXX, XXX−XXX

of the axial thiolate ligand in our {FeNO}^{6} series does NOT lead to the established inverse correlation of the Fe−NO and N−O vibrational frequencies, implying that the variation in the thiolate ligand does not significantly alter the Fe^{II}−NO^+ π back-bond. Instead, *the direct correlation observed here implies that there is a change in the Fe−NO σ-bond and, hence, that the axial thiolate imparts a σ-trans effect on the Fe−N−O unit.* In order to further characterize the nature of this σ interaction, we performed DFT calculations, as described in the next section.

Interestingly, the obtained slope of 1.20 (±0.31 is the standard error) from the linear fit in Figure 11A suggests that the thiolate's donor strength has close to a proportional effect in decreasing both the Fe−NO and N−O stretching frequencies (on an absolute wavenumber scale), with a slightly greater effect on the N−O stretching frequency. However, comparison of the relative percent change of the Fe−NO and N−O stretching frequencies of the six complexes, as shown in Figure 11B, paints a different picture. From this comparison, the total variation observed for the Fe−NO stretching frequency (~3%) is seen to be about 3 times larger than the total percentage change observed for the N−O stretching frequency (~1%). This suggests that the thiolate's donor strength actually has a greater effect on modulating the Fe−NO bond in heme-thiolate {FeNO}^{6} complexes in comparison to the N−O bond, which further supports the involvement of a thiolate σ-trans effect on the Fe−N−O unit to explain the experimental trend.

Computational Insight into the Nature of the Thiolate Trans Effect. With the new experimental trend in hand, we then reinvestigated the Fe−N−O bonding in {FeNO}^{6} complexes using DFT calculations. Here, we invoked (a) the [Fe(TPP)(Cl)(NO)] complex, which has slightly weaker Fe−NO and N−O bonds in comparison to imidazole-bound complexes with no trans effect,[21,24,64,65] (b) our thiophenolate complexes, and (c) a hypothetical sulfide complex, $[Fe(P)(S)(NO)]^-$. For all of these calculations, the porphine dianion (P^{2-}) was used as the porphyrin ligand.

The optimized structure of the chloro complex [Fe(P)(Cl)(NO)] is shown in Figure 12 (top left). Importantly, this compound shows a linear Fe−N−O unit (in agreement with the crystal structure of [Fe(TPP)(Cl)(NO)]),[24] which

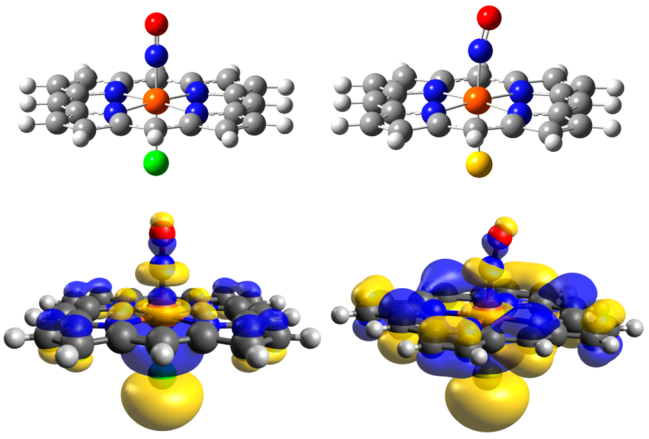

Figure 12. (top) DFT optimized (BP86/TZVP) structures of [Fe(P)(Cl)(NO)] (left) and $[Fe(P)(S)(NO)]^-$ (right). (bottom) MO contour plots that show the admixture of the Fe−N−O σ-antibonding (σ^*) orbital into the occupied (bonding) $Cl(p_z)\_d_{z^2}$ (left) and $S(p_z)\_d_{z^2}$ (right) MOs, respectively.

indicates that the σ-trans effect of the anionic ligand, here chloride, is not responsible for the bending of the Fe−N−O unit as originally proposed.[21,64] However, as previously proposed, our new results show again the mixing of an Fe−N−O antibonding (σ^*) orbital into the $Cl(p_z)$ donor orbital, mediated by the empty d_{z^2} orbital of the iron center. The resulting, occupied molecular orbital (MO), labeled $Cl(p_z)\_d_{z^2}$, is shown in Figure 12 (bottom left). This orbital is strongly Fe−NO and weakly N−O antibonding, which explains the experimental observation that the Fe−NO bond is more strongly affected by changes in the donor strength of the axial thiolate ligand in comparison to the N−O bond (see Figure 13). We further investigated whether the changes in the

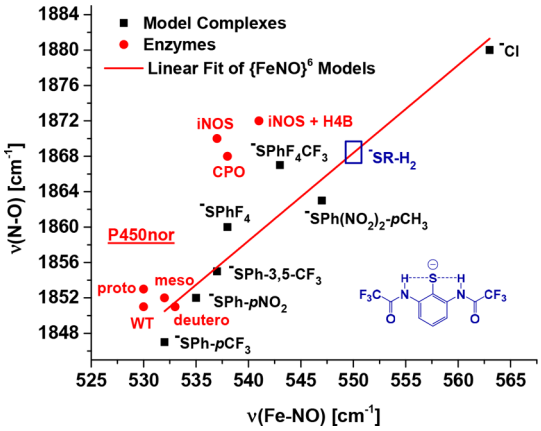

Figure 13. Correlation plot comparing the experimentally determined ν(Fe−NO) and ν(N−O) stretching frequencies of our {FeNO}^{6} model complexes and the NO adducts of ferric heme-thiolate enzymes. Note the data point for [Fe(TPP)(Cl)(NO)] added at the top right (ν(Fe−NO) 563 cm^{-1} and ν(N−O) 1880 cm^{-1}).[24] A slope of 0.99(±0.14) represents the best linear fit of the data for the six synthetic heme-thiolate and the TPP chloro {FeNO}^{6} complexes. The blue box represents a data point estimate for the $SR\text{-}H_2^-$ (=S-2,6-$(CF_3CONH)_2C_6H_3$, structure shown on the bottom right) {FeNO}^{6} complex, on the basis of the correlation line, giving an estimated ν(N−O) ~1870 cm^{-1} (±5 cm^{-1}).

Fe−NO and N−O bond strengths in [Fe(P)(Cl)(NO)] do indeed correlate with the amount of Fe−N−O (σ^*) character that is mixed into the $Cl(p_z)\_d_{z^2}$ MO. For this purpose, we fixed the Fe−Cl distance in [Fe(P)(Cl)(NO)] at different values larger and smaller than the optimized Fe−Cl bond length and then reoptimized the structure. As is evident from Table S1, a *decrease* in the Fe−Cl distance causes a weakening of both the Fe−NO and N−O bonds (and a lowering of the corresponding stretching frequencies), and, at the same time, an increase in the admixture of Fe−N−O (σ^*) character into $Cl(p_z)\_d_{z^2}$ is observed. The opposite trend is observed when the Fe−Cl distance is *increased* from the optimized value. These results therefore confirm the previous observation that the σ-trans effect of the axial anionic ligand is indeed mediated by back-bonding into the Fe−N−O antibonding σ^* orbital, which in turn is proportional to the donor strength of the anionic ligand bound trans to NO.

Since in all of the structures obtained for the [Fe(P)(Cl)(NO)] system the Fe−N−O unit remains linear, this poses the question then of what causes the bending of the Fe−N−O unit in the thiolate coordinated complexes. In order to determine whether this requires an anisotropic π donation from the axial ligand, we then investigated the hypothetical, sulfide-bound

DOI: 10.1021/acs.inorgchem.9b00091
Inorg. Chem. XXXX, XXX, XXX−XXX

complex [Fe(P)(S)(NO)]$^-$. Surprisingly, although sulfide is an isotropic π donor like chloride, the Fe−N−O unit is bent in the optimized structure of this complex, as shown in Figure 12 (top right). The shape of the Fe−N−O antibonding (σ^*) orbital is slightly different in this case, as shown in Figure 12 (bottom right) due to the Fe−N−O bending, but the fundamental nature of this orbital being strongly Fe−NO and weakly N−O antibonding remains. On the basis of these results, we conclude that the bending of the Fe−N−O unit is likely caused by strong π donation from the axial anionic ligand. Due to the fact that iron is in the ferrous low-spin state in heme {FeNO}^{6} complexes (due to their Fe^{II}−NO$^+$ type electronic structure), this causes strong Coulomb repulsion between the occupied ligand π and Fe(d_π) orbitals, which is decreased by mixing of one of the d_π orbitals with d_{z^2}, which effectively leads to a rotation of the d_π orbital and a bending of the Fe−N−O unit in the corresponding plane. On the other hand, for an anisotropic π-donor such as a thiolate, one would then predict that the Fe−N−O unit should bend more or less in the plane of the thiolate π-donor lone pair.

In summary, our results show that the σ-trans effect and the bending of the Fe−N−O unit in thiolate-coordinated heme {FeNO}^{6} complexes have two different origins that can be traced back to two different orbital interactions. With respect to the bonding properties of the Fe−N−O unit, the trans effect mediated by the σ^* orbital of the Fe−N−O unit is the more important interaction for the electronic structure of the heme {FeNO}^{6} complexes.

DISCUSSION

In this work, we accomplished the synthesis and characterization of the first series of heme-thiolate {FeNO}^{6} complexes where the donor strength of the thiolate is systematically varied. This was achieved using [Fe(TPP)(SPh*)] type complexes with a series of thiophenolate ligands (SPh*$^-$) that carry different electron-withdrawing substituents, according to Scheme 1. The five-coordinate high-spin ferric precursor complexes were first characterized using different spectroscopic methods and then reacted with NO gas at −80 °C. Here, the application of such low temperatures is key in order to obtain the corresponding NO adducts of type [Fe(TPP)(SPh*)(NO)], which decompose to the five-coordinate ferrous nitrosyl complex [Fe(TPP)(NO)] upon warming above −60 °C. Still, our studies also show that when more highly donating thiophenolates are used, such as the base compound SPh$^-$, then the thiolate either becomes more reactive toward NO than the iron center (forming a nitrosothiol), or the NO adduct decomposes immediately via homolytic Fe−S bond cleavage (see Scheme 2). In any case, a stable {FeNO}^{6} complex cannot be formed, even at −80 °C. Nevertheless, using six fluoro- and nitro-substituted thiophenolates, we were able to generate the first series of thiolate-coordinated heme {FeNO}^{6} complexes and determine their Fe−NO and N−O stretching frequencies. Our data demonstrate experimentally, for the first time, that the thiolate donor strength directly controls the strength of the Fe−NO and N−O bonds in the {FeNO}^{6} complexes. Here, as shown in Figure 13, a *direct* correlation of the Fe−NO and N−O bond strengths is observed as a function of the thiolate donor strength. Since the heme {FeNO}^{6} complexes are best described as Fe^{II}−NO$^+$ systems, where the Fe−NO interaction is dominated by π back-bonding, one would a priori expect that the thiolate ligand modulates the strength of the Fe−NO π back-bond. Despite this electronic structure, however, the observed direct correlation of the Fe−NO and N−O bond strengths rules out this possibility and demonstrates that the thiolate ligand does NOT modulate the Fe−NO π back-bond (since this would lead to an inverse correlation of the Fe−NO and N−O vibrational frequencies and, hence, bond strengths). Our results therefore directly support previous computational results which show that the strong σ donicity of the thiolate (and other axial anionic ligands bound trans to NO) leads to the occupation of an Fe−N−O σ-antibonding (σ^*) orbital and that the degree to which this orbital becomes occupied (via mixing into the thiolate(p_z)_d_{z^2} bonding MO) directly correlates with the donor strength of the trans-thiolate ligand. In other words, the thiolate imparts a σ-trans effect (or interaction, since it is a thermodynamic effect) on the bound nitrosyl ligand and, in this way, is able to control the degree of activation of the FeNO unit for P450nor catalysis.

Figure 13 shows additional protein data superimposed on our ν(N−O)/ν(Fe−NO) correlation plot, including the P450nor, CPO, and iNOS {FeNO}^{6} complexes. As is evident from this figure, the vibrational properties observed for our model complexes are reasonably well matched with the protein data. The small deviations observed in the plot are likely due to variations in the positioning of hydrogen bonds to the axial cysteinate, differences in heme conformation, electrostatic and steric effects, etc. between the different proteins, whereas, on the other hand, our data are all derived from electron-poor thiophenolates with the same heme coligand, in the same relative electrostatic environment. Importantly, the experimental data show that it is actually the [Fe(TPP)(SPh-*p*CF$_3$)(NO)] complex with the most electron rich thiolate in our series that exhibits the best agreement with the vibrational properties of the {FeNO}^{6} complex of P450nor and, hence, constitutes an excellent electronic model for the enzyme. In this regard, it should also be noted that the data point for the ferric NO adduct of P450nor is located very close to the correlation line. Thus, the prediction from DFT in this regard is incorrect. Notably, it has recently been highlighted that CPO shows much stronger hydrogen bonds to its axial cysteinate ligand in comparison to typical Cyt P450 enzymes and, thus, has a weaker thiolate donor in comparison to Cyt P450s.[13] The same is true for NOS enzymes, which have a highly conserved tryptophan residue that makes a strong H-bond to the proximal cysteinate.[28] Thus, the fact that the CPO and NOS {FeNO}^{6} complexes have higher N−O and Fe−NO stretching frequencies in comparison to those of P450nor is in full agreement with the results obtained for our {FeNO}^{6} complexes. In conclusion, the characterization of the model complexes presented in this work shows clearly that it is in fact the thiolate donor strength that is a major factor in dictating the N−O and Fe−NO bond strengths in heme-thiolate {FeNO}^{6} complexes and, hence, provides a means of how nature can control the electronic structure and the degree of activation of the Fe−N−O unit in these types of species. Furthermore, the fact that we can model the electronic effects of the hydrogen bonds to the Cys ligand in heme-thiolate proteins with electron-poor thiolates further confirms that the main electronic effect of the hydrogen bonds in the proteins is indeed a reduction of the donor strength of the axial thiolate (Cys) ligand.

Vice versa, this also means that NO can serve as a sensitive probe to measure the thiolate trans effect and, hence, thiolate donor strength in a model complex or a new Cyt P450 enzyme,

DOI: 10.1021/acs.inorgchem.9b00091
Inorg. Chem. XXXX, XXX, XXX−XXX

which is not possible in any other direct way. This could be accomplished by simply reacting the ferric form of the enzyme or model complex with NO (at low temperature, in the case of an inorganic complex) and then measuring the Fe−NO and N−O stretching frequencies as demonstrated here. A comparison of these data with the correlation plot in Figure 13 then provides a direct measure for the donor strength of the thiolate in the new system. This approach can be directly demonstrated for the only structurally characterized thiolate-coordinated $\{FeNO\}^6$ complex, $[Fe(OEP)(SR\text{-}H_2)(NO)]$ ($SR\text{-}H_2^-$ = S-2,6-$(CF_3CONH)_2C_6H_3$; OEP^{2-} = octaethylporphyrin dianion), where $SR\text{-}H_2^-$ is a thiophenolate ligand that is stabilized by two intramolecular amide hydrogen bonds.[30] In the initial communication, the N−O stretch of this complex was reported to be about 1850 cm^{-1}, which would match very well with that reported for the $\{FeNO\}^6$ complex of Cyt P450nor, making it an excellent model for the enzyme.[30] However, a closer inspection of the IR data provided in the paper shows that no well-defined signal was obtained for the N−O stretch in the IR spectrum of this complex (due to its instability).[30] Hence, the N−O stretch of this complex is not really known. On the other hand, the Fe−NO stretch for this complex has been accurately determined to be 549 cm^{-1} by resonance Raman spectroscopy.[31] As indicated in Figure 13, applying an Fe−NO stretch of about 550 cm^{-1} to the correlation line predicts the N−O stretch of this complex to actually occur around 1870 cm^{-1}. This result indicates that the two hydrogen bonds of $SR\text{-}H_2^-$ are too strong, greatly reducing the thiolate donor strength of the $SR\text{-}H_2^-$ ligand outside of the biologically relevant range of Cyt P450 enzymes. In other words, $[Fe(OEP)(SR\text{-}H_2)(NO)]$ is not a great electronic model for Cyt P450s. On the plus side, the two hydrogen bonds present in the $SR\text{-}H_2^-$ ligand greatly contribute to the stability of the corresponding heme-thiolate complexes, making this an attractive model system on the basis of stability.

In summary, our work provides fundamental insight into the nature of the thiolate σ-trans effect, which we propose is of general importance in Cyt P450 chemistry. By adjusting the strength of the hydrogen bonds, Nature is able to accurately fine tune the donor strength of the thiolate, which directly affects the electronic properties of the FeNO unit in the corresponding $\{FeNO\}^6$ complexes. In our work, we show that the same tuning of the Fe−NO and N−O bonds can be accomplished using electron-poor thiophenolate donors. On the other hand, the bending of the Fe−N−O unit is caused by the strong π donation of the thiolate; thus, this effect has a different orbital origin. Since the donor strength of the thiolate affects the FeNO unit, the question arises whether the σ-trans effect of the thiolate could be the underlying orbital interaction that is responsible for the so-called "push effect", first proposed by Dawson.[15] The idea is that the strong donicity of the proximal cysteinate ligand would assist in cleaving the O−O bond in the ferric-hydroperoxo intermediate (called "Compound 0") of Cyt P450 catalysis, in comparison to the analogous species in globins and other histidine-coordinated proteins. We used DFT calculations to obtain insight into this issue. First, we optimized the structure of the Cyt P450 model $[Fe(P)(SPh)(OOH)]^-$, but in this case no population of an Fe−O−O σ antibonding (σ^*) orbital is observed. However, it is also known that Compound 0 is further protonated in order to induce O−O bond cleavage. We therefore constructed a model of Compound 0 that is protonated at the distal O atom, $[Fe(P)(SPh)(OOH_2)]$. The optimized structure of this model

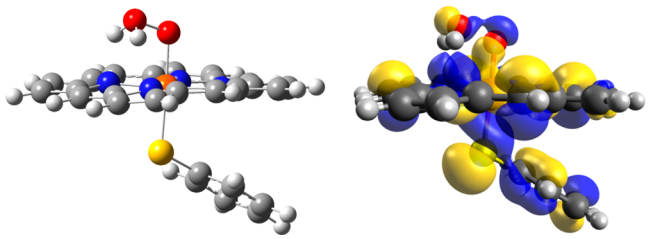

Figure 14. (left) DFT-optimized structure of $[Fe(P)(SPh)(OOH_2)]$. (right) MO contour plot that shows the admixture of the Fe−O−O σ antibonding (σ^*) orbital into the (occupied) Fe−S σ bonding MO (see the Experimental Section for additional details).

is shown in Figure 14 (left). Excitingly, in this case, we indeed observe the admixture of an Fe−O−O σ^* orbital into the σ-bonding MO between the $S(p_z)$ and Fe(d) orbitals, $S(p_z)\_d$, as shown in Figure 14 (right).

Hence, the σ-trans effect described here and quantified using NO as a probe provides an electronic−structural explanation for Dawson's push effect and, therefore, provides further validation that this is a real electronic effect. Importantly, this also means that Nature can control the magnitude of the push effect in an ideal way via adjustment of the hydrogen-bonding network to the proximal cysteinate ligand of Cyt P450s. This explains why typical Cyt P450 monooxygenases have overall weaker hydrogen bonds to the thiolate or, in other words, stronger cysteinate donors in comparison to P450nor. This manifests itself in lower N−O stretching frequencies of 1800−1820 cm^{-1} for Cyt P450 monoxygenases in comparison to ν(N−O) of 1851 cm^{-1} in P450nor. In this indirect way, the vibrational data of the $\{FeNO\}^6$ complexes, which measure the donor strength of the thiolate, also serve as a sensitive probe for the magnitude of the "push" effect in Cyt P450 monooxygenase enzymes.

■ ASSOCIATED CONTENT

Supporting Information

The Supporting Information is available free of charge on the ACS Publications website at DOI: 10.1021/acs.inorgchem.9b00091.

Additional spectroscopic characterization of the ferric thiolate precursor complexes, NO reactivity data for all complexes, EPR data and fits, and coordinates of DFT-optimized structures (PDF)

■ AUTHOR INFORMATION

Corresponding Author

*E-mail for N.L.: lehnertn@umich.edu.

ORCID

Andrew P. Hunt: 0000-0003-0565-9050

Nicolai Lehnert: 0000-0002-5221-5498

Notes

The authors declare no competing financial interest.

■ ACKNOWLEDGMENTS

This work was supported by a grant from the National Science Foundation (CHE-1464696 to N.L.). We thank Dr. Hannah Shafaat and Dr. Anastasia Manesis from The Ohio State University for granting us access to their resonance Raman spectrometer and for their assistance in the data collection.

DOI: 10.1021/acs.inorgchem.9b00091
Inorg. Chem. XXXX, XXX, XXX−XXX

REFERENCES

(1) Bredt, D. S.; Snyder, S. H. Nitric Oxide: A Physiologic Messenger Molecule. *Annu. Rev. Biochem.* **1994**, *63*, 175−195.

(2) Vincent, J.-L.; Zhang, H.; Szabo, C.; Preiser, J.-C. Effects of Nitric Oxide in Septic Shock. *Am. J. Respir. Crit. Care Med.* **2000**, *161*, 1781−1785.

(3) Lehnert, N.; Berto, T. C.; Galinato, M. G. I.; Goodrich, L. E. In *Handbook of Porphyrin Science*; World Scientific: 2010; pp 1−247.

(4) Daiber, A.; Shoun, H.; Ullrich, V. Nitric oxide reductase (P450nor) from Fusarium oxysporum. *J. Inorg. Biochem.* **2005**, *99*, 185−193.

(5) Shimizu, H.; Obayashi, E.; Gomi, Y.; Arakawa, H.; Park, S. Y.; Nakamura, H.; Adachi, S.-i.; Shoun, H.; Shiro, Y. Proton delivery in NO reduction by fungal nitric-oxide reductase: Cryogenic crystallography, spectroscopy, and kinetics of ferric-NO complexes of wild-type and mutant enzymes. *J. Biol. Chem.* **2000**, *275*, 4816−4826.

(6) US EPA Overview of Greenhouse Gases [Online Early Access]; published online 2016; https://www.epa.gov/ghgemissions/overview-greenhouse-gases.

(7) Riplinger, C.; Bill, E.; Daiber, A.; Ullrich, V.; Shoun, H.; Neese, F. New Insights into the Nature of Observable Reaction Intermediates in Cytochrome P450 NO Reductase by Using a Combination of Spectroscopy and Quantum Mechanics/Molecular Mechanics Calculations. *Chem. - Eur. J.* **2014**, *20*, 1602−1614.

(8) Higgins, S. A.; Welsh, A.; Orellana, L. H.; Konstantinidis, K. T.; Chee-Sanford, J. C.; Sanford, R. A.; Schadt, C. W.; Löffler, F. E. Detection and Diversity of Fungal Nitric Oxide Reductase Genes (p450nor) in Agricultural Soils. *Appl. Environ. Microbiol.* **2016**, *82*, 2919−2928.

(9) Novinscak, A.; Goyer, C.; Zebarth, B. J.; Burton, D. L.; Chantigny, M. H.; Filion, M. Novel P450nor Gene Detection Assay Used To Characterize the Prevalence and Diversity of Soil Fungal Denitrifiers. *Appl. Environ. Microbiol.* **2016**, *82*, 4560−4569.

(10) Chen, H.; Shi, W. Opening up the N_2O-producing fungal community in an agricultural soil with a cytochrome p450nor-based primer tool. *Applied Soil Ecology* **2017**, *119*, 392−395.

(11) McQuarters, A. B.; Wolf, M. W.; Hunt, A. P.; Lehnert, N. 1958−2014: After 56 Years of Research, Cytochrome P450 Reactivity Is Finally Explained. *Angew. Chem., Int. Ed.* **2014**, *53*, 4750−4752.

(12) Denisov, I. G.; Makris, T. M.; Sligar, S. G.; Schlichting, I. Structure and Chemistry of Cytochrome P450. *Chem. Rev.* **2005**, *105*, 2253−2278.

(13) Krest, C. M.; Silakov, A.; Rittle, J.; Yosca, T. H.; Onderko, E. L.; Calixto, J. C.; Green, M. T. Significantly shorter Fe−S bond in cytochrome P450-I is consistent with greater reactivity relative to chloroperoxidase. *Nat. Chem.* **2015**, *7*, 696.

(14) Galinato, M. G. I.; Spolitak, T.; Ballou, D. P.; Lehnert, N. Elucidating the Role of the Proximal Cysteine Hydrogen-Bonding Network in Ferric Cytochrome P450cam and Corresponding Mutants Using Magnetic Circular Dichroism Spectroscopy. *Biochemistry* **2011**, *50*, 1053−1069.

(15) Sono, M.; Roach, M. P.; Coulter, E. D.; Dawson, J. H. Heme-Containing Oxygenases. *Chem. Rev.* **1996**, *96*, 2841−2888.

(16) Yosca, T. H.; Rittle, J.; Krest, C. M.; Onderko, E. L.; Silakov, A.; Calixto, J. C.; Behan, R. K.; Green, M. T. Iron(IV)hydroxide pKa and the Role of Thiolate Ligation in C−H Bond Activation by Cytochrome P450. *Science* **2013**, *342*, 825−829.

(17) Shiro, Y.; Fujii, M.; Iizuka, T.; Adachi, S. i.; Tsukamoto, K.; Nakahara, K.; Shoun, H. Spectroscopic and Kinetic Studies on Reaction of Cytochrome P450nor with Nitric Oxide: Implication for its Nitric Oxide Reduction Mechanism. *J. Biol. Chem.* **1995**, *270*, 1617−1623.

(18) Oshima, R.; Fushinobu, S.; Su, F.; Zhang, L.; Takaya, N.; Shoun, H. Structural Evidence for Direct Hydride Transfer from NADH to Cytochrome P450nor. *J. Mol. Biol.* **2004**, *342*, 207−217.

(19) Lehnert, N.; Praneeth, V. K. K.; Paulat, F. Electronic structure of iron(II)−porphyrin nitroxyl complexes: Molecular mechanism of fungal nitric oxide reductase (P450nor). *J. Comput. Chem.* **2006**, *27*, 1338−1351.

(20) Enemark, J. H.; Feltham, R. D. Principles of structure, bonding, and reactivity for metal nitrosyl complexes. *Coord. Chem. Rev.* **1974**, *13*, 339−406.

(21) Paulat, F.; Lehnert, N. Electronic Structure of Ferric Heme Nitrosyl Complexes with Thiolate Coordination. *Inorg. Chem.* **2007**, *46*, 1547−1549.

(22) Praneeth, V. K. K.; Paulat, F.; Berto, T. C.; George, S. D.; Näther, C.; Sulok, C. D.; Lehnert, N. Electronic Structure of Six-Coordinate Iron(III)-Porphyrin NO Adducts: The Elusive Iron(III)-NO(radical) State and Its Influence on the Properties of These Complexes. *J. Am. Chem. Soc.* **2008**, *130*, 15288−15303.

(23) Soldatova, A. V.; Ibrahim, M.; Olson, J. S.; Czernuszewicz, R. S.; Spiro, T. G. New Light on NO Bonding in Fe(III) Heme Proteins from Resonance Raman Spectroscopy and DFT Modeling. *J. Am. Chem. Soc.* **2010**, *132*, 4614−4625.

(24) McQuarters, A. B.; Kampf, J. W.; Alp, E. E.; Hu, M.; Zhao, J.; Lehnert, N. Ferric Heme-Nitrosyl Complexes: Kinetically Robust or Unstable Intermediates? *Inorg. Chem.* **2017**, *56*, 10513−10528.

(25) Obayashi, E.; Tsukamoto, K.; Adachi, S. i.; Takahashi, S.; Nomura, M.; Iizuka, T.; Shoun, H.; Shiro, Y. Unique Binding of Nitric Oxide to Ferric Nitric Oxide Reductase from Fusarium oxysporum Elucidated with Infrared, Resonance Raman, and X-ray Absorption Spectroscopies. *J. Am. Chem. Soc.* **1997**, *119*, 7807−7816.

(26) Hu, S.; Kincaid, J. R. Resonance Raman characterization of nitric oxide adducts of cytochrome P450cam: the effect of substrate structure on the iron-ligand vibrations. *J. Am. Chem. Soc.* **1991**, *113*, 2843−2850.

(27) Hu, S.; Kincaid, J. R. Heme active-site structural characterization of chloroperoxidase by resonance Raman spectroscopy. *J. Biol. Chem.* **1993**, *268*, 6189−6193.

(28) Couture, M.; Adak, S.; Stuehr, D. J.; Rousseau, D. L. Regulation of the Properties of the Heme-NO Complexes in Nitric-oxide Synthase by Hydrogen Bonding to the Proximal Cysteine. *J. Biol. Chem.* **2001**, *276*, 38280−38288.

(29) Li, D.; Stuehr, D. J.; Yeh, S. R.; Rousseau, D. L. Heme Distortion Modulated by Ligand-Protein Interactions in Inducible Nitric-oxide Synthase. *J. Biol. Chem.* **2004**, *279*, 26489−26499.

(30) Xu, N.; Powell, D. R.; Cheng, L.; Richter-Addo, G. B. The first structurally characterized nitrosyl heme thiolate model complex. *Chem. Commun.* **2006**, 2030−2032.

(31) Goodrich, L. E.; Paulat, F.; Praneeth, V. K. K.; Lehnert, N. Electronic Structure of Heme-Nitrosyls and Its Significance for Nitric Oxide Reactivity, Sensing, Transport, and Toxicity in Biological Systems. *Inorg. Chem.* **2010**, *49*, 6293−6316.

(32) Suzuki, N.; Higuchi, T.; Urano, Y.; Kikuchi, K.; Uchida, T.; Mukai, M.; Kitagawa, T.; Nagano, T. First Synthetic NO-Heme-Thiolate Complex Relevant to Nitric Oxide Synthase and Cytochrome P450nor. *J. Am. Chem. Soc.* **2000**, *122*, 12059−12060.

(33) Adler, A. D.; Longo, F. R.; Kampas, F.; Kim, J. On the preparation of metalloporphyrins. *J. Inorg. Nucl. Chem.* **1970**, *32*, 2443−2445.

(34) Tsai, R.; Yu, C. A.; Gunsalus, I. C.; Peisach, J.; Blumberg, W.; Orme-Johnson, W. H.; Beinert, H. Spin-State Changes in Cytochrome P-450cam on Binding of Specific Substrates. *Proc. Natl. Acad. Sci. U. S. A.* **1970**, *66*, 1157−1163.

(35) Tang, S. C.; Koch, S.; Papaefthymiou, G. C.; Foner, S.; Frankel, R. B.; Ibers, J. A.; Holm, R. H. Axial ligation modes in iron(III) porphyrins. Models for the oxidized reaction states of cytochrome P-450 enzymes and the molecular structure of iron(III) protoporphyrin IX dimethyl ester p-nitrobenzenethiolate. *J. Am. Chem. Soc.* **1976**, *98*, 2414−2434.

(36) Li, J.; Peng, Q.; Oliver, A. G.; Alp, E. E.; Hu, M. Y.; Zhao, J.; Sage, J. T.; Scheidt, W. R. Comprehensive Fe−Ligand Vibration Identification in {FeNO}6 Hemes. *J. Am. Chem. Soc.* **2014**, *136*, 18100−18110.

(37) Kobayashi, H.; Higuchi, T.; Kaizu, Y.; Osada, H.; Aoki, M. Electronic Spectra of Tetraphenylporphinatoiron(III) Methoxide. *Bull. Chem. Soc. Jpn.* **1975**, *48*, 3137−3141.

DOI: 10.1021/acs.inorgchem.9b00091
Inorg. Chem. XXXX, XXX, XXX−XXX

(38) Miller, K. M.; Strouse, C. E. Two-dimensional short-range order in the crystal structure of (tetraphenylporphinato)iron(III) 2,3,5,6-tetrafluorobenzenethiolate. Analysis of the x-ray diffuse scattering and a simulation of crystal growth. *Inorg. Chem.* **1984**, *23*, 2395−2400.
(39) Oshio, H.; Ama, T.; Watanabe, T.; Nakamoto, K. Iron·sulfur vibrations in model compounds of cytochromes P-450 and c. *Inorg. Chim. Acta* **1985**, *96*, 61−66.
(40) Arasasingham, R. D.; Balch, A. L.; Cornman, C. R.; De Ropp, J. S.; Eguchi, K.; La Mar, G. N. Proton NMR studies of iron(III) porphyrins with axial phenoxide or thiophenoxide ligands. *Inorg. Chem.* **1990**, *29*, 1847−1850.
(41) Collman, J. P.; Sorrell, T. N.; Hoffman, B. M. Models for cytochrome P-450. *J. Am. Chem. Soc.* **1975**, *97*, 913−914.
(42) Collman, J. P.; Sorrell, T. N.; Hodgson, K. O.; Kulshrestha, A. K.; Strouse, C. E. Molecular dynamics in the solid state. A dynamic model of the low-spin iron(III) to high-spin iron(III) transformation in P450 enzymes. *J. Am. Chem. Soc.* **1977**, *99*, 5180−5181.
(43) Byrn, M. P.; Strouse, C. E. Porphyrin sponges. Inversion disorder and inversion twinning in lattice clathrates based on five-coordinate metallotetraarylporphyrin complexes. *J. Am. Chem. Soc.* **1991**, *113*, 2501−2508.
(44) Goodrich, L. E. Model Complexes of Cytochrome P450 Nitric Oxide Reductase. Ph.D. Dissertation, University of Michigan, 2012.
(45) Das, P. K.; Samanta, S.; McQuarters, A. B.; Lehnert, N.; Dey, A. Valence tautomerism in synthetic models of cytochrome P450. *Proc. Natl. Acad. Sci. U. S. A.* **2016**, *113*, 6611−6616.
(46) Frisch, M. J.; Trucks, G. W.; Schlegel, H. B.; Scuseria, G. E.; Robb, M. A.; Cheeseman, J. R.; Scalmani, G.; Barone, V.; Mennucci, B.; Petersson, G. A.; Nakatsuji, H.; Caricato, M.; Li, X.; Hratchian, H. P.; Izmaylov, A. F.; Bloino, J.; Zheng, G.; Sonnenberg, J. L.; Hada, M.; Ehara, M.; Toyota, K.; Fukuda, R.; Hasegawa, J.; Ishida, M.; Nakajima, T.; Honda, Y.; Kitao, O.; Nakai, H.; Vreven, T.; Montgomery, J. A., Jr.; Peralta, J. E.; Ogliaro, F.; Bearpark, M.; Heyd, J. J.; Brothers, E.; Kudin, K. N.; Staroverov, V. N.; Kobayashi, R.; Normand, J.; Raghavachari, K.; Rendell, A.; Burant, J. C.; Iyengar, S. S.; Tomasi, J.; Cossi, M.; Rega, N.; Millam, J. M.; Klene, M.; Knox, J. E.; Cross, J. B.; Bakken, V.; Adamo, C.; Jaramillo, J.; Gomperts, R.; Stratmann, R. E.; Yazyev, O.; Austin, A. J.; Cammi, R.; Pomelli, C.; Ochterski, J. W.; Martin, R. L.; Morokuma, K.; Zakrzewski, V. G.; Voth, G. A.; Salvador, P.; Dannenberg, J. J.; Dapprich, S.; Daniels, A. D.; Farkas, O.; Foresman, J. B.; Ortiz, J. V.; Cioslowski, J.; Fox, D. J. *Gaussian 09*; Gaussian, Inc.: Wallingford, CT, 2009.
(47) Becke, A. D. Density-functional exchange-energy approximation with correct asymptotic behavior. *Phys. Rev. A: At., Mol., Opt. Phys.* **1988**, *38*, 3098−3100.
(48) Perdew, J. P. Density-functional approximation for the correlation energy of the inhomogeneous electron gas. *Phys. Rev. B: Condens. Matter Mater. Phys.* **1986**, *33*, 8822−8824.
(49) Schäfer, A.; Huber, C.; Ahlrichs, R. Fully optimized contracted Gaussian basis sets of triple zeta valence quality for atoms Li to Kr. *J. Chem. Phys.* **1994**, *100*, 5829−5835.
(50) Neese, F. The ORCA program system. *Wiley Interdisciplinary Reviews: Computational Molecular Science* **2012**, *2*, 73−78.
(51) Li, H.; Igarashi, J.; Jamal, J.; Yang, W.; Poulos, T. L. Structural studies of constitutive nitric oxide synthases with diatomic ligands bound. *JBIC, J. Biol. Inorg. Chem.* **2006**, *11*, 753−768.
(52) Meininger, D. J.; Caranto, J. D.; Arman, H. D.; Tonzetich, Z. J. Studies of Iron(III) Porphyrinates Containing Silanethiolate Ligands. *Inorg. Chem.* **2013**, *52*, 12468−12476.
(53) Bohle, D. S.; Goodson, P. A.; Smith, B. D. Synthesis, structure and ligand exchange reactions of Ru(TTP)(NO)(OMe). *Polyhedron* **1996**, *15*, 3147−3150.
(54) Addison, A. W.; Stephanos, J. J. Nitrosyliron(III) hemoglobin: autoreduction and spectroscopy. *Biochemistry* **1986**, *25*, 4104−4113.
(55) Hoshino, M.; Maeda, M.; Konishi, R.; Seki, H.; Ford, P. C. Studies on the Reaction Mechanism for Reductive Nitrosylation of Ferrihemoproteins in Buffer Solutions. *J. Am. Chem. Soc.* **1996**, *118*, 5702−5707.
(56) Roncaroli, F.; Videla, M.; Slep, L. D.; Olabe, J. A. New features in the redox coordination chemistry of metal nitrosyls {M−NO+; M−NO; M−NO-(HNO)}. *Coord. Chem. Rev.* **2007**, *251*, 1903−1930.
(57) Ellison, M. K.; Scheidt, W. R. Synthesis, Molecular Structures, and Properties of Six-Coordinate [Fe(OEP)(L)(NO)]$^+$ Derivatives: Elusive Nitrosyl Ferric Porphyrins. *J. Am. Chem. Soc.* **1999**, *121*, 5210−5219.
(58) Abucayon, E. G.; Khade, R. L.; Powell, D. R.; Zhang, Y.; Richter-Addo, G. B. Hydride Attack on a Coordinated Ferric Nitrosyl: Experimental and DFT Evidence for the Formation of a Heme Model−HNO Derivative. *J. Am. Chem. Soc.* **2016**, *138*, 104−107.
(59) Abucayon, E. G.; Khade, R. L.; Powell, D. R.; Shaw, M. J.; Zhang, Y.; Richter-Addo, G. B. Over or under: hydride attack at the metal versus the coordinated nitrosyl ligand in ferric nitrosyl porphyrins. *Dalton Transactions* **2016**, *45*, 18259−18266.
(60) Wang, J.; Rousseau, D. L.; Abu-Soud, H. M.; Stuehr, D. J. Heme coordination of NO in NO synthase. *Proc. Natl. Acad. Sci. U. S. A.* **1994**, *91*, 10512−10516.
(61) Franke, A.; Stochel, G.; Suzuki, N.; Higuchi, T.; Okuzono, K.; van Eldik, R. Mechanistic Studies on the Binding of Nitric Oxide to a Synthetic Heme-Thiolate Complex Relevant to Cytochrome P450. *J. Am. Chem. Soc.* **2005**, *127*, 5360−5375.
(62) Weichsel, A.; Maes, E. M.; Andersen, J. F.; Valenzuela, J. G.; Shokhireva, T. K.; Walker, F. A.; Montfort, W. R. Heme-assisted S-nitrosation of a proximal thiolate in a nitric oxide transport protein. *Proc. Natl. Acad. Sci. U. S. A.* **2005**, *102*, 594−599.
(63) Spiro, T. G.; Wasbotten, I. H. CO as a vibrational probe of heme protein active sites. *J. Inorg. Biochem.* **2005**, *99*, 34−44.
(64) Xu, N.; Goodrich, L. E.; Lehnert, N.; Powell, D. R.; Richter-Addo, G. B. Preparation of the Elusive [(por)Fe(NO)(O-ligand)] Complex by Diffusion of Nitric Oxide into a Crystal of the Precursor. *Angew. Chem., Int. Ed.* **2013**, *52*, 3896−3900.
(65) Xu, C.; Spiro, T. G. Ambidentate H-bonding by heme-bound NO: structural and spectral effects of − O versus − N H-bonding. *JBIC, J. Biol. Inorg. Chem.* **2008**, *13*, 613−621.
(66) Pérez-González, A.; Castañeda-Arriaga, R.; Verastegui, B.; Carreón-González, M.; Alvarez-Idaboy, J. R.; Galano, A. Estimation of empirically fitted parameters for calculating pKa values of thiols in a fast and reliable way. *Theor. Chem. Acc.* **2018**, *137*, 5.
(67) Hupe, D. J.; Pohl, E. R. A Demonstration of the Reactivity—Selectivity Principle for the Thiol—Disulfide Interchange Reaction. *Isr. J. Chem.* **1985**, *26*, 395−399.
(68) Horn, M.; Nienhaus, K.; Nienhaus, G. Fourier transform infrared spectroscopy study of ligand photodissociation and migration in inducible nitric oxide synthase. *F1000Research* **2014**, *3*, 290.
(69) Singh, U. P.; Obayashi, E.; Takahashi, S.; Iizuka, T.; Shoun, H.; Shiro, Y. The effects of heme modification on reactivity, ligand binding properties and iron-coordination structures of cytochrome P450nor. *Biochim. Biophys. Acta, Protein Struct. Mol. Enzymol.* **1998**, *1384*, 103−111.

DOI: 10.1021/acs.inorgchem.9b00091
Inorg. Chem. XXXX, XXX, XXX−XXX